IVYSPRING INTERNATIONAL PUBLISHER

Theranostics

2018; 8(18): 5039-5058. doi: 10.7150/thno.26981

Research Paper

Increased recruitment of endogenous stem cells and chondrogenic differentiation by a composite scaffold containing bone marrow homing peptide for cartilage regeneration

Jiaju Lu[1*], Xuezhen Shen[2*], Xun Sun[2], Heyong Yin[3], Shuhui Yang[1], Changfeng Lu[2], Yu Wang[2], Yifan Liu[1], Yingqi Huang[1], Zijin Yang[1], Xianqi Dong[1], Chenhao Wang[1], Quanyi Guo[2], Lingyun Zhao[1], Xiaodan Sun[1], Shibi Lu[2], Antonios G. Mikos[4], Jiang Peng[2]✉, and Xiumei Wang[1]✉

1. State Key Laboratory of New Ceramics and Fine Processing, Key Laboratory of Advanced Materials of Ministry of Education, School of Materials Science and Engineering, Tsinghua University, Beijing 100084, China
2. Institute of Orthopedics, Chinese PLA General Hospital, Beijing 100853, China
3. Experimental Surgery and Regenerative Medicine, Department of Surgery, Ludwig-Maximilians-University, Munich 80336, Germany
4. Department of Bioengineering, Bioscience Research Collaborative, Rice University, Texas 77030, USA

* Contributed equally to this work

✉ Corresponding author: Xiumei Wang, E-mail: wxm@mail.tsinghua.edu.cn, Phone: 86-10-62782966. Fax: 86-10-62771160. Jiang Peng, pengjiang301@126.com

Received: 2018.05.01; Accepted: 2018.08.27; Published: 2018.10.05

Abstract

Even small cartilage defects could finally degenerate to osteoarthritis if left untreated, owing to the poor self-healing ability of articular cartilage. Stem cell transplantation has been well implemented as a common approach in cartilage tissue engineering but has technical complexity and safety concerns. The stem cell homing-based technique emerged as an alternative promising therapy for cartilage repair to overcome traditional limitations. In this study, we constructed a composite hydrogel scaffold by combining an oriented acellular cartilage matrix (ACM) with a bone marrow homing peptide (BMHP)-functionalized self-assembling peptide (SAP). We hypothesized that increased recruitment of endogenous stem cells by the composite scaffold could enhance cartilage regeneration.

Methods: To test our hypothesis, *in vitro* proliferation, attachment and chondrogenic differentiation of rabbit mesenchymal stem cells (MSCs) were tested to confirm the bioactivities of the functionalized peptide hydrogel. The composite scaffold was then implanted into full-thickness cartilage defects on rabbit knee joints for cartilage repair, in comparison with microfracture or other sample groups. Stem cell recruitment was monitored by dual labeling with CD29 and CD90 under confocal microcopy at 1 week after implantation, followed by chondrogenic differentiation examined by qRT-PCR. Repaired tissue of the cartilage defects was evaluated by histological and immunohistochemistry staining, microcomputed tomography (micro-CT) and magnetic resonance imaging (MRI) at 3 and 6 months post-surgery. Macroscopic and histological scoring was done to evaluate the optimal *in vivo* repair outcomes of this composite scaffold.

Results: The functionalized SAP hydrogels could stimulate rabbit MSC proliferation, attachment and chondrogenic differentiation during *in vitro* culture. At 7 days after implantation, increased recruitment of MSCs based on $CD29^+$ /$CD90^+$ double-positive cells was found *in vivo* in the composite hydrogel scaffold, as well as upregulation of cartilage-associated genes (aggrecan, Sox9 and type II collagen). After 3 and 6 months post-surgery, the articular cartilage defect in the composite scaffold-treated group was fully covered with cartilage-like tissue with a smooth surface, which was similar to the surrounding native cartilage, according to the results of histological and immunohistochemistry staining, micro-CT and MRI analysis. Macroscopic and histological scoring confirmed that the quality of cartilage repair was significantly improved with implantation of the composite scaffold at each timepoint, in comparison with microfracture or other sample groups.

Conclusion: Our findings demonstrated that the composite scaffold could enhance endogenous stem cell homing and chondrogenic differentiation and significantly improve the therapeutic outcome of chondral defects. The present study provides a promising approach for *in vivo* cartilage repair without cell

transplantation. Optimization of this strategy may offer great potential and benefits for clinical application in the future.

Key words: self-assembling peptide hydrogel, acellular cartilage matrix, stem cell homing, cartilage regeneration

Introduction

The restoration of articular cartilage defects is still a great clinical challenge because of the poor intrinsic healing potential of cartilage tissue [1, 2]. Most patients who suffer from full-thickness articular cartilage defects may have degenerative changes and eventually progress to osteoarthritis, a leading source of disability worldwide [3]. Stem cell-based therapy has been one of the most promising treatments for cartilage injury, but many problems remains, such as the restrictive availability of stem cell sources, low viability, technical complexity with high medical costs, and the ethical and safety concerns of clinical translation [4]. Recently, cell homing-based treatment by recruiting endogenous stem cells to the site of injury has opened a new avenue for *in situ* tissue regeneration [5, 6].

For cartilage repair, few stem cells are resident in the adult articular cartilage, and stem cells from other sources are unable to readily arrive at the defects via the blood supply [7]. Microfracture (MF), as the first-line treatment, has been widely performed to access the endogenous MSC populations from the bone marrow, which serve as an ideal autologous cell source for articular cartilage repair [8]. However, long-term studies have shown that its clinical outcomes remain unsatisfactory [9]. The blood clots by MF usually result in scar formation and fibrocartilage, which are inferior to normal hyaline cartilage [10, 11]. The reasons for the failure fall into three categories: (i) low numbers of endogenous stem cells due to the inadequate capability of recruiting stem cells by MF [12]; (ii) inefficient chondrogenic differentiation of recruited stem cells [13]; (iii) unsuitable microenvironment for chondrocytes and stem cells because of load-bearing forces and fluid movement of blood clots [14, 15]. Hence, there is a tremendous need to develop ideal biomaterials that are capable of serving as powerful artificial niches to recruit, program, and direct host cells *in situ* for tissue regeneration purposes.

Meng *et al*. prepared demineralized bone matrix particles by applying chitosan hydrogel for cartilage engineering, which was suitable for proliferation and chondrogenesis of rat bone marrow-derived MSCs [16, 17]. To provide a better microenvironment for MSCs and chondrocytes, Zheng *et al.* previously reported a three-dimensional (3D) acellular scaffold derived from natural cartilage extracellular matrix (ECM) employed in cartilage regeneration [18]. The acellular cartilage matrix (ACM) scaffold not only has similar biochemical composition to the natural articular cartilage ECM, but is fabricated to mimic cartilage physiological morphology with its well oriented structure. *In vitro* and *in vivo* studies demonstrated that the ACM scaffold could provide a feasible microenvironment for MSC attachment, proliferation and differentiation into chondrocytes [19]. However, oriented ACM scaffold with capacity for recruiting stem cells has been rarely reported.

The functional peptide sequence PFS (PFSSTKT) is identified as the bone marrow homing peptide (BMHP) through a phage display technology, and it has the ability to home to bone marrow and bind to stem cells [20, 21]. In our group, a functionalized self-assembling peptide (SAP) was designed and prepared by introducing the functional motif PFS to the parent SAP RADA16-I (RAD, Ac-$(RADA)_4$-NH_2) [22]. The SAP solutions have the ability to self-assemble into nanofibers and then form a 3D hydrogel under physiological conditions [23]. Several studies reported that the SAP hydrogel scaffold could provide a beneficial microenvironment for chondrocytes and MSCs and enhance the synthesis of cartilage-like ECM [24-26]. Therefore, in this study we applied the functionalized SAP mixtures RAD/PFS hydrogel containing BMHP to modify the ACM scaffold in order to promote cartilage regeneration based on the strategy of stem cell homing by recruiting more endogenous mesenchymal stem cells and promoting their chondrogenic differentiation.

In summary, we combined the oriented ACM scaffold with the RAD/PFS to form a composite hydrogel scaffold, ACM+RAD/PFS, that was designed to mend the microenvironment of the defect for cartilage regeneration by exerting the advantages of these two scaffolds. The composite scaffold was applied to repair full-thickness articular cartilage defects in a rabbit model. Endogenous stem cell recruitment and chondrogenic differentiation in the composite scaffold were examined. The cartilage repair effect was then evaluated by micro-CT, MRI, and gross and histological analysis.

Methods

Peptide synthesis and sample preparation

RAD solution (1% w/v, 10 mg/mL) was

purchased as BeaverNano™ from BeaverNano technology company, Suzhou, China. The designer functionalized peptide was prepared by solid-phase peptide synthesis via directly adding the bioactive bone marrow homing peptide PFS (PFSSTKT) to the C-terminus of RAD (ChinaPeptides Co.,Ltd, Shanghai, China). It was dissolved in Milli-Q water at a final concentration of 1% w/v, sonicated for 15 min (VCX 130 PB, Sonics, CT) and then filter-sterilized with an Acrodisc Syringe Filter (0.2 μm HT Tuffrun membrane, Pall Corp., Ann Arbor, MI) for subsequent use. The designer peptide solutions were mixed at a volume ratio of 1:1 with 1% RAD solution to obtain the functionalized peptide mixtures, namely, RAD/PFS.

Circular dichroism (CD)

The CD measurements were performed as described by Lu *et al* [27]. Briefly, 200 μL of the sample solutions at a working concentration of 0.01% w/v were loaded into a 1 mm path-length quartz cuvette. An applied photophysics chirascan instrument (Leatherhead, UK) was used to collect its spectrum in 180–260 nm. Each spectrum was collected in triplicate. The calculation of molar ellipticity was based on the formula [28]: $[\theta]_\lambda = \theta_{obs} \times 1/(10Lcn)$, where $[\theta]_\lambda$ is the molar ellipticity at λ in deg·cm²·d/mol, θ_{obs} is the measured ellipticity in mdeg, L is the path length of the cell in cm, c is the concentration of peptide in M, and n is the number of amino acids in the peptide.

Atomic force microscopy (AFM)

The AFM measurements were performed as described by Lu *et al* [27]. Briefly, 5 μL of RAD or RAD/PFS solution at a working concentration of 0.01% (w/v) was dropped onto a freshly cleaved mica surface and left for 5 s, then rinsed twice with 100 μL of Milli-Q water. After air-drying overnight, the peptide samples were tested with an AFM (Bruker Dimension ICON, Billerica, MA, USA) in tapping mode. Images were recorded with a silicon scanning probe (FESP, Vecco Probe Inc., CA, USA) with a tip curvature radius of 10 nm and 225 μm length. The scanning area was 2 μm × 2 μm and the frequency was 1.00 Hz. Analysis of fiber diameters of peptides was performed using Image-Pro Plus 6.0 software (Media Cybernetics, Rockville, MD, USA).

ACM-oriented scaffold fabrication

The ACM scaffold was fabricated as previously described [18]. Briefly, cartilage slices from porcine femoral condyle were shattered and decellularized under aseptic conditions. Then, the decellularized cartilage microfilaments were prepared after pulverization and differential centrifugation. They were washed intensively with sterile phosphate buffered saline (PBS) and then made into a 3% w/v suspension in PBS. The suspension was placed into cylindrical molds, and the ACM-oriented scaffolds were fabricated by a simple freeze-drying and cross-linking technique. After sterilization by ^{60}Co irradiation at 5 mrad, the ACM-oriented scaffolds were stored at 4 °C for further use.

Composite hydrogel scaffold construction

The ACM-oriented scaffold as a cartilage explant was made into a cylinder with a 3-mm diameter and 1.5-mm height by using a sterile biopsy punch. 20 μL of the RAD or RAD/PFS peptide solution was added to the ACM-oriented scaffold. 50 μL of PBS was then layered on top of the peptide-modified ACM scaffold to initiate hydrogel self-assembly. After equilibrating the gel to physiological pH, the RAD and RAD/PFS peptide solution formed a hydrogel with the ACM-oriented scaffold, which were denoted as ACM+RAD and ACM+RAD/PFS.

Scanning electron microscopy (SEM)

ACM, ACM+RAD, and ACM+RAD/PFS were fixed with 2.5% glutaraldehyde for 2 h, washed twice in PBS, and subsequently dehydrated using a series of graded ethanol solutions, respectively. Once the peptide hydrogel scaffold was in 100% ethanol, the ethanol was dried using a CO_2 critical point dryer (Samdri-PVT-3D; Tousimis, Rockville, MD, USA). Upon CO_2 removal, peptide hydrogel scaffold was sputter-coated with platinum alloy and examined using a MERLIN VP compact microscope (Carl Zeiss, Jena, Germany) at 15 kV.

In vitro rabbit bone marrow-derived MSCs growth

Rabbit MSCs (Oricell™, Cyagen Biosciences, Inc.; Cat. No. RBXMX-01001) at passage four were used for *in vitro* evaluation. The cells were cultured in a complete medium (Oricell™, Cyagen Biosciences, Inc.; Cat. No. RBXMX-90011) composed of rabbit mesenchymal stem cell basal medium, 10% fetal bovine serum (FBS), 100 U/mL penicillin-streptomycin, L-glutamine (all from Cyagen Biosciences). 50 μL of peptide solution (pure RAD or functionalized peptide mixture RAD/PFS) was loaded directly into the wells of a 96-well plate and then 150 μL of culture medium was very carefully added onto the peptide solution for gelation. Once the hydrogel formed, the medium was carefully removed and changed twice to equilibrate the gel to physiological pH prior to plating the cells. Rabbit MSCs were seeded on the surface of peptide gels and tissue culture plate (TCP) control (5×10^3 cells/well, n=5). Fresh medium was changed every three days. Cell growth and proliferation in different groups were detected with Cell Counting

Kit-8 (CCK-8, DOJINDO, Japan) as described previously [27]. Briefly, at day 1, 3 and 5, the cultured cells were incubated with 10% CCK-8 working solution in cell culture medium for 2 h at 37 °C in the dark. Then, 100 μL of the supernatant was extracted to a new 96-well plate, and the absorbance at 450 nm was measured using an EnSpire Multimode Plate Reader (PerkinElmer, USA).

The *in vitro* cell recruitment capacity of MSCs was determined by assaying cell attachment to the peptide hydrogels as described previously [16, 29]. The desired number of sterilized culture plate inserts (10 mm-diameter, 0.4 mm Millicell-CM, Millipore, MA) were placed in a 24-well culture plate. 100 μL of peptide solution (pure RAD or functionalized peptide mixture RAD/PFS) was loaded directly into each of the inserts. Peptide scaffolds were prepared as described above [27]. Passage four rabbit MSCs (1×10^4) in 400 μL of medium was seeded on the surface of each peptide gel. After 3 and 7 days of incubation, the cell culture medium was carefully removed and the cells were rinsed with 0.01 M phosphate-buffered saline (PBS) three times. Then, the cells (n=3 in each group) were fixed with 2% paraformaldehyde (20 min at room temperature) and permeated with 0.1% Triton X-100 solution for 5 min. After having been washed with PBS, 1% bovine serum albumin (BSA) solution was added and the cells were then incubated for 30 min at room temperature. Finally, actin filaments and nuclei were then stained with Rhodamine-Phalloidin (1:300, Cytoskeleton, Cat# PHDR1, Cytoskeleton, Denver, CO, USA) and 5 μM SYTOX green nucleic acid stain (Invitrogen Molecular Probes, Inc.), respectively. The images were captured by a confocal laser scanning microscope (LSM 710, Carl Zeiss, Germany) at 20x magnification.

In vitro chondrogenic differentiation of MSCs on peptide gels

400 μL of peptide solution (pure RAD or functionalized peptide mixture RAD/PFS) was loaded directly into the wells of a 12-well plate and then 200 μL of culture medium was very carefully added onto the peptide solution for gelation. Once the hydrogel formed, the medium was carefully removed and changed twice to equilibrate the gel to physiological pH prior to plating the cells. Rabbit MSCs were seeded on the surface of the peptide gels and tissue culture plate (TCP) control (1×10^5 cells/well, n=3). At 24 h after cell seeding, the culture medium was changed with a chondrogenic induction medium (RBXMX-90041; CyagenBiosciences Inc., Santa Clara, CA, USA) that contained chondrogenic differentiation basal medium, 0.1 M dexamethasone, 40 μg/mL L-proline, 100 μg/mL sodium pyruvate, 1% ITS and supplement, ascorbate acid and 10 ng/mL TGF-β3 (all from Cyagen Biosciences), and incubated at 37 °C under 5% CO_2 condition. Fresh medium was changed every three days. After incubation for 7 and 14 days, total RNAs from the cell samples were isolated by miRNA kit (DP501, Tiangen, Beijing, China) and cDNAs were reverse transcribed using FastQuant RT Kit (KR-106, Tiangen, Beijing, China). Quantitative PCR was performed by the SYBR green method using iTaq SYBR Green Supermix (172-5122, Bio-Rad, Richmond, CA, USA) and the CFX96 real-time PCR detection system (Bio-Rad, Richmond, CA, USA). The real-time PCR conditions were as follows: 95 °C for 3 min, followed by 40 cycles of 95 °C for 10 s and 60 °C for 30 s. A melting curve analysis was added at the end of the amplification procedure. Non-specific amplification was not identified from the melting curves. The sequences of primers for GAPDH, type I collagen (Col1), type II collagen (Col2), Sox9 and aggrecan are listed in **Table S1**. Data are presented as the fold-change using the $2^{-\Delta\Delta Ct}$ method [30].

Animal experiment

All animals were treated according to the standard guidelines approved by the Institutional Animal Care and Use Committee at Chinese PLA General Hospital. Adult New Zealand white rabbits 3-6 months old weighing between 2.5 and 3.0 kg were randomly divided into 4 groups (MF, ACM, ACM+RAD, and ACM+RAD/PFS group) of 6 rabbits (n = 12 knees) per group for each timepoint, as shown in **Figure S1**. After intravenous injection with 3% sodium pentobarbital (40 mg/kg body weight), the rabbits' knee joints were opened with a medial parapatellar approach. A cylindrical full-thickness defect (3 mm in diameter × 1.5 mm depth) was created in the center of the trochlear groove of both knee joints using a sterile biopsy punch. Microfracture was performed routinely to mobilize the bone marrow in all groups. The ACM alone, ACM+RAD, and ACM+RAD/PFS groups (3 mm in diameter × 1.5 mm depth) were implanted into the articular cartilage defects, respectively. The MF groups were treated with microfracture operations alone as controls. All the implants were placed flush with the surface of the surrounding cartilage. After euthanasia at 1 week, 3 months and 6 months, knee joints from each group were harvested for further evaluation. A schematic illustration was drawn to introduce the experimental design and process, as shown in **Figure 1A**. And the preparation process of the composite scaffolds and the self-assembly of the functionalized SAP mixture are shown in **Figure 1B-C**.

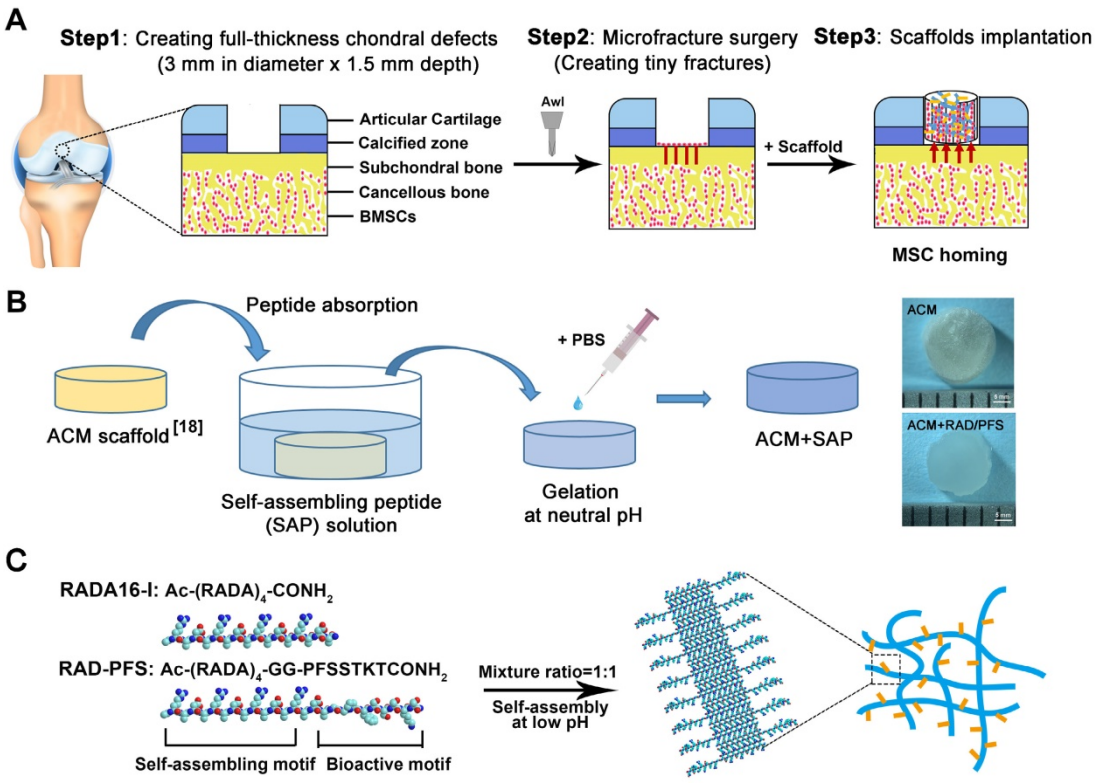

Figure 1. Animal experimental design **(A)**, a schematic illustration of the preparation process of the composite hydrogel system **(B)** and the functionalized self-assembling peptide RAD/PFS **(C)**.

Table 1. Primary and secondary antibodies used in this study

	Company	Cat #	Dilution
Primary antibody			
Collagen II	Novus Biologicals	NBP2-33343	1:100
CD29	Novus Biologicals	NB100-92076	1:100
CD90	Novus Biologicals	NB200-530	1:200
Secondary antibody			
Goat anti-mouse IgG	Novus Biologicals	NB7539	1:200
Goat anti-mouse IgG H&L	Abcam	ab150117	1:1000
Goat anti-rabbit IgG H&L	Abcam	ab150084	1:1000
4',6-diamidino-2-phenylindole (DAPI)	Life Technologies	D3571	1 μg/mL

Immunofluorescence staining

At one week after the operation, cylindrical tissue samples (3 mm in diameter and 1.5 mm in depth) from the defect site of all groups were harvested. All the details of primary and secondary antibodies used in this study are shown in **Table 1**. For immunofluorescence staining, the samples were fixed in 4% paraformaldehyde at room temperature for 30 min and then were exposed to microwave heating (95–100 °C for 15 min) in sodium citrate buffer (10 mM sodium citrate, pH 6.0) for target antigen retrieval. After being cooled at room temperature, the samples were blocked with 10% goat serum for 30 min, then incubated with primary antibodies against CD29 and CD90 (**Table 1**) at 4 °C overnight. After incubation with secondary antibodies for 1 h and DAPI for 10 min (**Table 1**) at room temperature, the central parts of the samples were directly observed under a Leica TCS SP8 confocal microscope (Leica Microsystems, Germany) and analyzed by Imaris 7.2.3 software (Bitplane, Zurich, Switzerland). Fifty Z-slices per image were collected and displayed as a maximum Z-projection. The specimens have a thickness of up to 50 μm (step: 1 μm). The total cell numbers and CD29 and CD90 doubly labeled cells were determined by Image pro plus 6.0 software (Media Cybernetics Inc., MD, USA) according to the maximum intensity projection images (**Figure S2**).

Quantitative real-time polymerase chain reaction (qRT-PCR)

Except for immunofluorescence staining, the residual samples were flash-frozen in liquid nitrogen and pulverized using a mortar. Total RNA was extracted by an RNeasy Mini kit (Qiagen, Hilden, Germany), and quantified using a Nucleic Acid and Protein Analyzer (Microfuge18; Beckman-Coulter). The cDNA was synthesized from 1 μg total RNA using an iScript™ cDNA Synthesis kit (Bio-Rad, Richmond, CA, USA). The sequence of primers for GAPDH, Col1, Col2, Sox9 and aggrecan are listed in **Table S1**. Reverse transcription was performed at 37 °C for 15 min and at 85 °C for 5 s using the ReverTra

Ace® qPCR RT Kit (FSQ-101, TOYOBO, Japan) following the manufacturer's protocol. qPCR was performed 5 min at 95 °C, followed by 40 cycles of 15 s at 95 °C, 15 s at 60 °C and 15 s at 72 °C. The process was performed using StepOne TM Real-Time PCR System (Applied Biosystems). The relative expressions were determined by normalizing expression of each Ct value to glyceraldehyde 3-phosphate dehydrogenase (GAPDH) Ct value. Three replicate samples were analyzed for each gene (n = 3). Data are presented as fold change using the $2^{-\Delta\Delta Ct}$ method [30].

MSCs isolation and identification

The isolation of rabbit MSCs was performed as described by Luo *et al* [31]. Briefly, four independent composite scaffolds ACM+RAD/PFS from defected joints 2 weeks after implantation were harvested. For tissue explant culture, the samples were washed three times with PBS (Gibco/Invitrogen, Carlsbad, CA, USA) supplemented with 1% penicillin/streptomycin (CyagenBiosciences Inc., Santa Clara, CA, USA), and cut into small pieces. The cell culture medium was replaced every three days and cells were expanded to passage 2 and collected for further experiments.

To characterize the isolated cells, the specific markers of MSCs were assessed by a PCR and electrophoresis method [32, 33]. The total RNA from isolated cells was extracted as described above. Target DNAs were amplified by using iTaq SYBR Green Supermix (172-5122, Bio-Rad, Richmond, CA, USA) and the CFX96 real-time PCR detection system (Bio-Rad, Richmond, CA, USA) using gene-specific primers such as CD29, CD34, CD44, CD45, CD90, CD105 (**Table S2**). GAPDH was used as internal control. The amplification process was as follows: 95 °C for 3 min, followed by 30 cycles of 95 °C for 10 s and 60 °C for 30 s. To confirm the absence of specific markers of MSCs, the PCR products were observed using an electrophoresis method on 2% (w/v) agarose gel and staining with ethidium bromide (Sigma, USA). Briefly, 10 µL of PCR product or DNA ladder was loaded into the sample well or ladder well. Then, gel electrophoresis was performed at a constant voltage of 100 V for 40 min in a 1× TAE buffer (40 mM Tris base, 40 mM glacial acetic acid, 1 mM ethylenediaminetetraacetic acid). The DNA was visualized with a Chemidoc XRS Gel Documentation System (Bio-Rad, Richmond, CA, USA). The product bands were analyzed by Gel-Pro Analyzer 3.1 software (Media Cybernetics, MD, USA).

The differentiation capacity of isolated MSCs into chondrocytes was evaluated using the chondrogenic induction medium (RBXMX-90041; CyagenBiosciences Inc., Santa Clara, CA, USA), which contained chondrogenic differentiation basal medium, 0.1 M dexamethasone, 40 µg/mL L-proline, 100 µg/mL sodium pyruvate, 1% ITS and supplement, ascorbate acid and 10 ng/mL TGF-β3 (all from Cyagen Biosciences). The cells were seeded on a 12-well culture plate (1×10^5 cells/well, n=3). After 7 days of culture in chondrogenesis medium, the expression of cartilage-specific proteoglycan was assessed by Alcian Blue (Cyagen Biosciences Inc., Santa Clara, CA, USA) staining. Briefly, cells were fixed in methanol for 15 min and then incubated with Alcian Blue for 30 min. Then, the excess stain was washed with Milli-Q water. Images were captured under a light microscope.

Microcomputed tomography analysis

At 3 and 6 months post-surgery, rabbit femur end samples from each group (n=4) were harvested and fixed in 4% w/v buffered paraformaldehyde for 2 days, mounted in a poly(methyl methacrylate) holder, and subjected to a General Electric (GE) eXplorer Locus SP (GE Healthcare, USA) using previously established methods [34]. GE Health Care MicroView ABA 2.1.2 software was used to reconstruct and analyze the image data in axial, coronal, and sagittal planes. A cylindrical region of interest 3 mm in diameter and 1.5 mm in thickness corresponding to the original defect location was selected for further analysis. The bone mineral density (BMD) and bone volume fraction (BVF) were then assessed.

Magnetic resonance imaging analysis

At 3 and 6 months post-surgery, MRI was performed on a 7.0 T MRI system (Bruker, PharmaScan; Bruker BioSpin, Germany) using a 38-mm knee coil, following a previously described protocol [35]. The T2 mapping sequence was acquired using the following imaging parameters as previously described [29]: time of repetition (TR) of 1000 ms, time of echo (TE) of 13.8 ms, 227 bandwidth (BW, Hz/pixel), 180° flip angle, 80 mm field of view , 512 × 256 matrix, 2 mm slice thickness with 20% distance factor. T2 relaxation times from a sagittal slice through the center of the cartilage repair site were calculated using the Bruker ParaVision 5.0 system.

Gross and histological analysis

At 3 and 6 months post-surgery, the animals were euthanized. The knee samples in each group were dissected and examined macroscopically by three independent (blinded) examiners, using the International Cartilage Repair Society (ICRS) grading system (**Table S3**) [36]. After gross examination, specimens were decalcified in 10% w/v ethylenediamine-tetraacetic acid (EDTA, pH=7.4) for 6 weeks at 37 °C. They were dehydrated by

immersion in a series of ethanol solutions (70%, 80%, 85%, 90%, 95%, and 100%) and xylene solutions in ethanol (50% and 100%). Specimens were then processed in paraffin wax and cut into slices with an approximate thickness of 7 μm. The sections were subsequently stained with hematoxylin and eosin (H&E), Sirius red (SR), Safranin O/Fast Green and toluidine blue (TB). For immunohistochemical staining of Col2, sections were immersed in 0.25% pepsin at 37 °C for 20 min and blocked in 10% goat serum. Following antigen retrieval, the sections were incubated with primary antibodies against Col2 at 4 °C overnight. After rinsing with PBS, they were incubated with goat anti-mouse IgG for 1 h. Finally, they were immersed for 2-5 min in Tris-HCl buffer containing 0.05% DAB and 0.005% hydrogen peroxide. Each section was scanned using a Zeiss Axio Scan Z1 slide scanner (Carl Zeiss Microscopy GmbH, Jena, Germany). Representative images were cropped and processed using ZenBlue software. The sections from 6 knee samples per group were blindly and independently scored by three evaluators, according to the Wakitani Score for defective cartilage (**Table S4**) [37].

Statistical analysis

All values are expressed as mean ± standard deviation (SD). An SPSS 23.0 software package (SPSS Inc., Chicago, IL, USA) was used for all statistical procedures. Statistical analysis of the data was carried out using *t*-test for independent samples or one-way analysis of variance (ANOVA) for multi-group comparisons, followed by Tukey's HSD post hoc test (equal variances) or Dunnett's T3 post hoc test (unequal variances). Differences were considered statistically significant when the *p*-value was less than 0.05.

Results

Preparation and characterization of the composite scaffold

Firstly, we investigated the structural properties of the functionalized peptide solutions. In order to characterize the secondary structure, CD spectra were obtained. A typical spectrum for β-sheet structures with a maximum molar ellipticity at 195 nm and a minimum at 216 nm was observed for RAD and RAD/PFS peptide solutions (**Figure 2A**). However, the intensity of molar ellipticity for RAD/PFS was less than that for RAD, due to the addition of the functional peptide motif PFS (**Figure 2A**). We then used AFM to analyze the formation of nanofibers of each peptide solution. The presence of interwoven nanofibers in both RAD and RAD/PFS solutions was observed (**Figure 2B**). The uniform and long nanofibers were randomly distributed on the mica surface with functionalized peptide mixtures RAD/PFS solution, which suggested that the functionalized peptides interact with RAD and incorporate into the nanofibers quite well. By adding and exchanging cell culture medium or PBS, these high densities of nanofibers could undergo gelation into a hydrogel under physiological condition (pH = ~7, temperature = 37 °C). Gros photographs of RAD and RAD/PFS hydrogels are shown in **Figure 2C**. After gelation, SEM was performed. These results also confirmed the self-assembling nanofiber formation in both RAD and RAD/PFS peptide hydrogels (**Figure 2D**).

The ACM scaffold was fabricated by an improved decellularization method, which could preserve most of the components of healthy cartilage, such as glycosaminoglycans (GAGs) and Col2 [18]. The SEM images of the cross section of ACM clearly show an interconnected porous structure that is uniformly distributed throughout the scaffold. Moreover, the SEM images of the vertical sections indicated that the ACM had well-oriented porous channels, as shown in the **Figure 2E**. The composite scaffold of ACM and SAP hydrogels was prepared by introducing peptide solutions to the ACM scaffold, and then the addition of cell culture medium or PBS promoted the process of peptide self-assembly and gelation. Compared with the gross observation of ACM, the composite scaffold combining peptide hydrogels had a smoother surface and looked like a piece of gel (**Figure 1B**). Although the oriented structure of ACM was affected to a certain extent after combining with SAP, the oriented features were still observed in the ACM+RAD and ACM+RAD/PFS groups from the vertical section view (**Figure 2E**).

In vitro effects of RAD/PFS peptide gels on rabbit MSCs

The results of CCK-8 assay (**Figure 3A**) showed that the cell proliferation of the rabbit MSCs increased with culture time, especially after 3 days of culture on the peptide scaffolds. The optical density (OD) values of the RAD/PFS peptide gel were significantly higher than those of the control group RAD gel at each timepoint, indicating the excellent biocompatibilities and bioactivity of RAD/PFS peptide hydrogel for cell attachment and growth.

MSC affinity to the peptide hydrogel was tested with a cell attachment assay. The typical morphologies of rabbit MSCs after 3 and 7 days of cell culture on the surface of different peptide gels in a regular growth medium are shown in **Figure 3B**. It was noted that the rabbit MSCs grown on the

RAD/PFS peptide gels had good attachment and spread after 3 and 7 days of culture, showing typical fusiform MSC morphology. By contrast, the rabbit MSCs on the surface of RAD peptide gels showed poor adhesion at each timepoint. After 7 days *in vitro* culture, there were significantly more MSCs on RAD/PFS peptide gel scaffolds than RAD peptide hydrogel scaffolds (**Figure 3B**). In addition, the rabbit MSCs on the RAD/PFS peptide hydrogel showed a significant cluster due to its specific MSC homing capacity.

The chondrogenesis of rabbit MSCs grown on the surfaces of different peptide scaffolds was also evaluated by qRT-PCR (**Figure 5**). The expressions of the chondrogenic genes (aggrecan, Sox9 and Col2) of the RAD/PFS group were significantly higher than those of the RAD groups after 7 and 14 days of chondrogenic induction. There was no significant difference in the expression of Col1 after 7 days of culture between the TCP, RAD and RAD/PFS groups. Although the expression of osteogenic gene (Col1) slightly increased in the RAD/PFS group after 14 days of culture, it was much lower than that of aggrecan, Sox9 and Col2 (**Figure 4**).

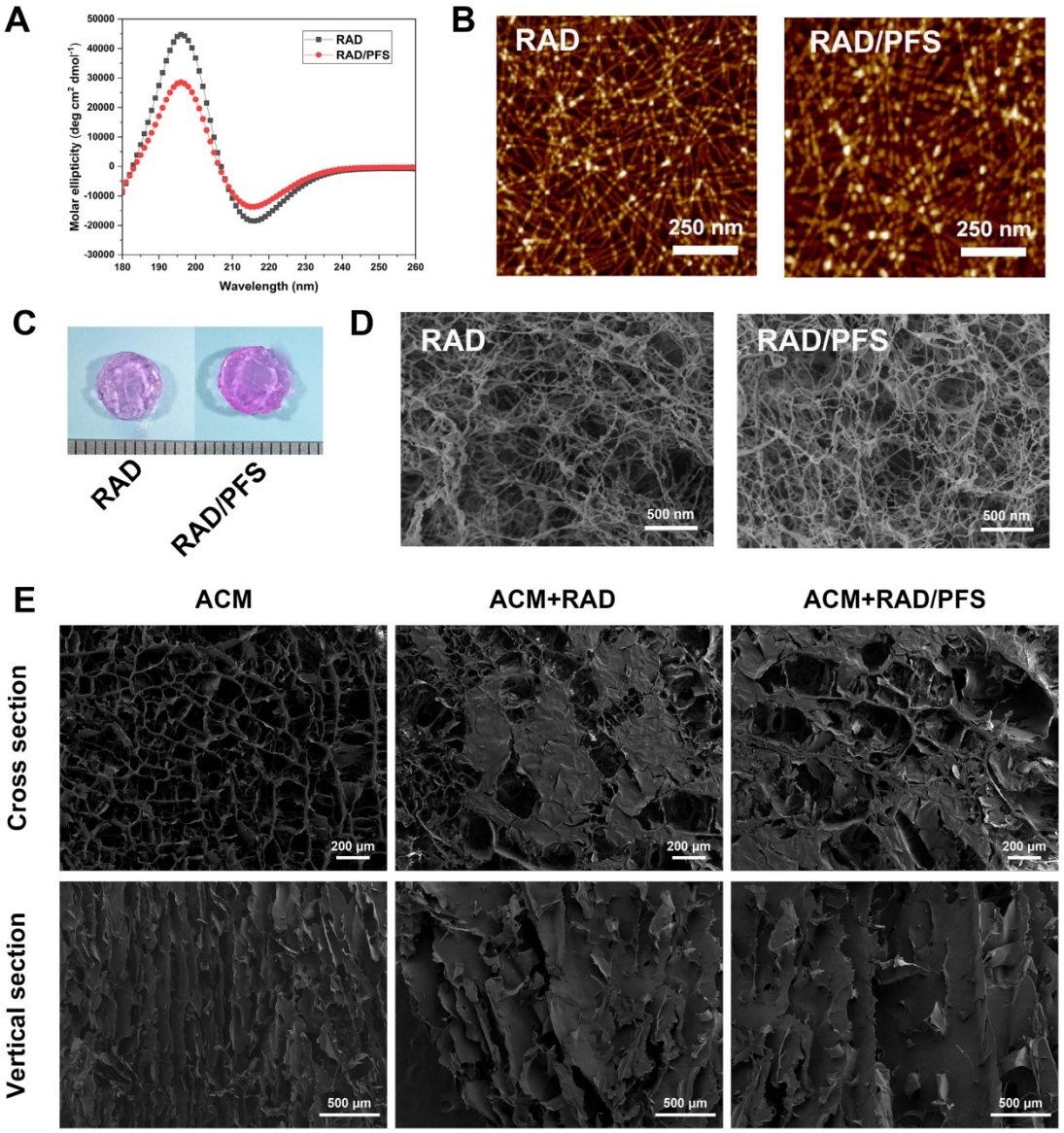

Figure 2. Structural characterization of self-assembling peptide hydrogels and the composite scaffolds. (A) Typical CD spectrum of RAD and RAD/PFS peptide solutions. **(B)** AFM images of RAD and RAD/PFS peptide solutions (scale bars: 250 nm). **(C)** Gross morphology of RAD and RAD/PFS peptide hydrogels. **(D)** SEM images of RAD and RAD/PFS peptide hydrogels (scale bars: 500 nm). **(E)** SEM characterization of ACM alone, ACM+RAD, and ACM+RAD/PFS composite scaffolds. Scale bars: 200 μm (cross section); 500 μm (vertical section).

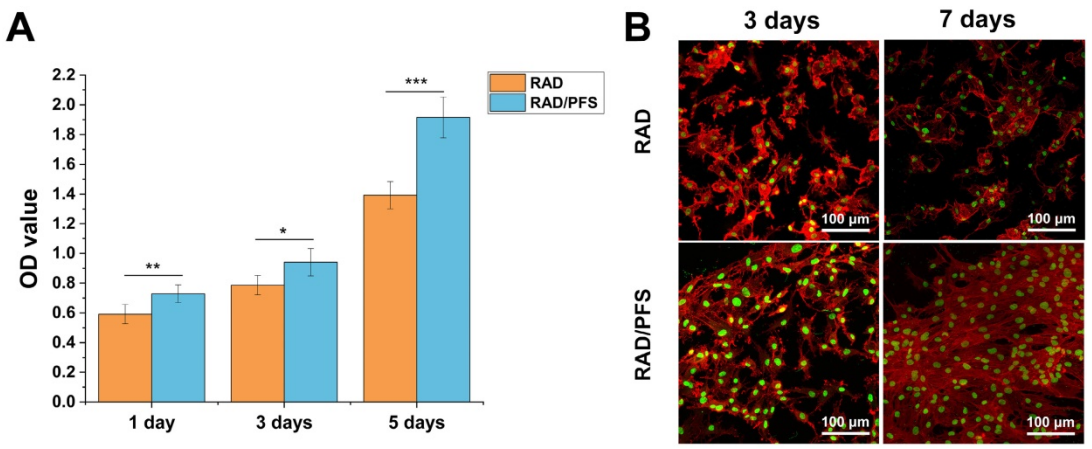

Figure 3. ***In vitro*** **proliferation and attachment of rabbit MSCs grown on the RAD and RAD/PFS peptide gels. (A)** The CCK-8 assay was performed after 1, 3 and 5 days of cell culture (n = 5). Mean ± SD; $^{*}p < 0.05$, $^{**}p < 0.01$ and $^{***}p < 0.001$. **(B)** Typical morphologies of rabbit MSCs grown on the peptide gel scaffolds after 3 and 7 days of culture. The cells were stained with rhodamine-phalloidin (red) and Sytox green (green).

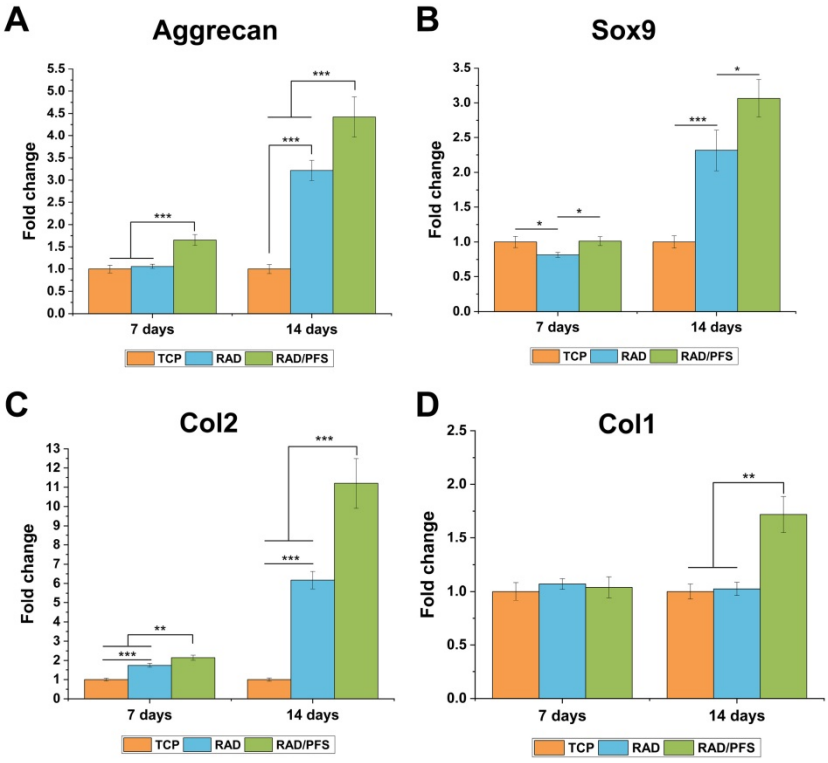

Figure 4. The chondrogenic differentiation of rabbit MSCs on the TCP control group, RAD and RAD/PFS gels, respectively. The expression of cartilage-specific genes, (**A**) Aggrecan, (**B**) Sox9 and (**C**) Col2, and osteogenic gene, (**D**) Col1 (n = 3) were detected by qRT-PCR. Mean ± SD; $^{*}p < 0.05$, $^{**}p < 0.01$ and $^{***}p < 0.001$.

These results suggest that the RAD/PFS peptide hydrogel scaffold could promote rabbit MSCs attachment, proliferation, and chondrogenic differentiation.

MSCs recruitment *in vivo*

To assess the ability of the composite scaffolds to recruit MSCs *in vivo*, cylindrical tissue samples from the defect site were harvested 1 week after implantation. The central parts of the samples were directly examined by confocal laser scanning microscopy with immunofluorescence staining.

MSCs have been defined as positive for the stem cell markers CD29, CD44, CD90, and CD105, and negative for the hematopoietic stem cell marker CD34, and the panleukocyte marker CD45 [38, 39]. A large number of studies have already demonstrated that MSCs highly express CD29 and CD90 [40-43]. Recently, Kim et al. identified MSCs by dual labeling with CD29 and CD44 antibodies [44]. Here the cells in the samples were also subjected to dual-labeling with CD29 and CD90 antibodies to indicate the existence of MSCs.

As shown in **Figure 5**, more $CD29^{+}$ or $CD90^{+}$ cells

were observed in the ACM+RAD and ACM+RAD/PFS groups compared with the MF and ACM alone groups. Moreover, the merge images showed relatively more $CD29^+/CD90^+$ cells in the ACM+RAD/PFS group than in the other three groups (**Figure 5**).

The ACM+RAD/PFS group recruited significantly more $CD29^+/CD90^+$ cells (1462 ± 10^6 per mm^2) than all other groups (**Figure 6A**, $p < 0.001$). The cell number of $CD29^+/CD90^+$ cells in the ACM+RAD group (522 ± 84 per mm^2) was similar to that in the ACM group (581 ± 94 per mm^2), which was significantly more than that in the MF group (263 ± 67 per mm^2) (**Figure 6A**, $p < 0.05$).

To confirm the existence of the recruited MSCs in the implanted scaffolds, cylindrical tissue samples from the defect site of the RAD/PFS group were harvested and cut into small pieces for tissue explant culture at 2 weeks after implantation. The specific markers of MSCs including CD29, CD34, CD44, CD45, CD90, and CD105 were assessed by a PCR and electrophoresis method [32, 33]. As shown in **Figure S3**, The isolated MSCs at passage 2 were positive for CD29, CD44, CD90 and CD105, but negative for CD34, and CD45, which were consistent with the expression of surface antigen of MSCs according to the definition of MSCs [38]. Moreover, these isolated cells at passage 2 could still be successfully induced towards chondrogenic differentiation *in vitro* (**Figure S4**).

Taken together, the composite scaffold RAD/PFS could promote MSCs recruitment and migration into the scaffold.

Chondrogenic differentiation of recruited MSCs

To investigate the chondrogenic differentiation or dedifferentiation of recruited MSCs *in vivo*, total RNA was extracted and subjected to qRT-PCR at 1 week after surgery. The chondrogenesis markers (aggrecan, Sox9 and Col2) and osteogenesis markers (Col1) were tested for mRNA expression (**Figure 6B-F**).

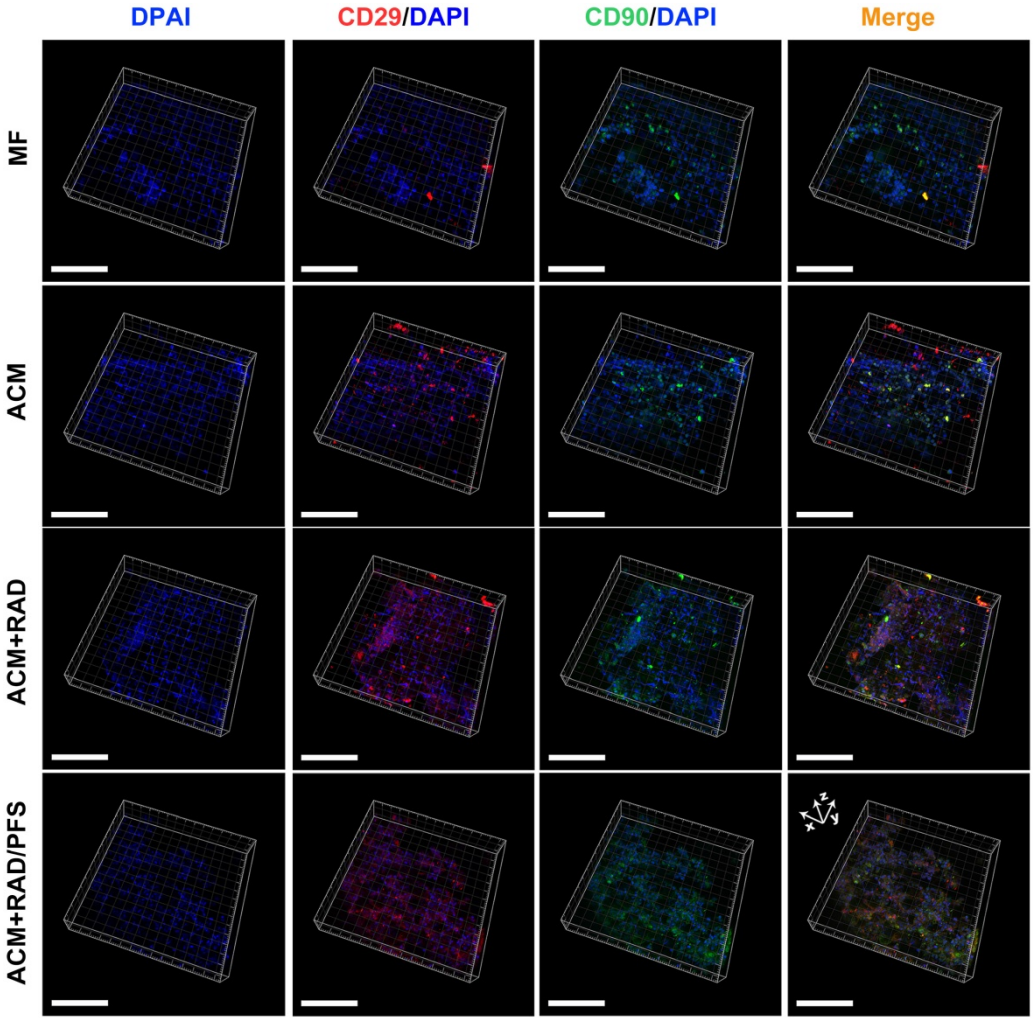

Figure 5. Identification of *in vivo* MSC homing to different scaffolds at 1 week after implantation. Immunostained images representing MSC identification at the center of the scaffolds (scale bars: 100 μm).

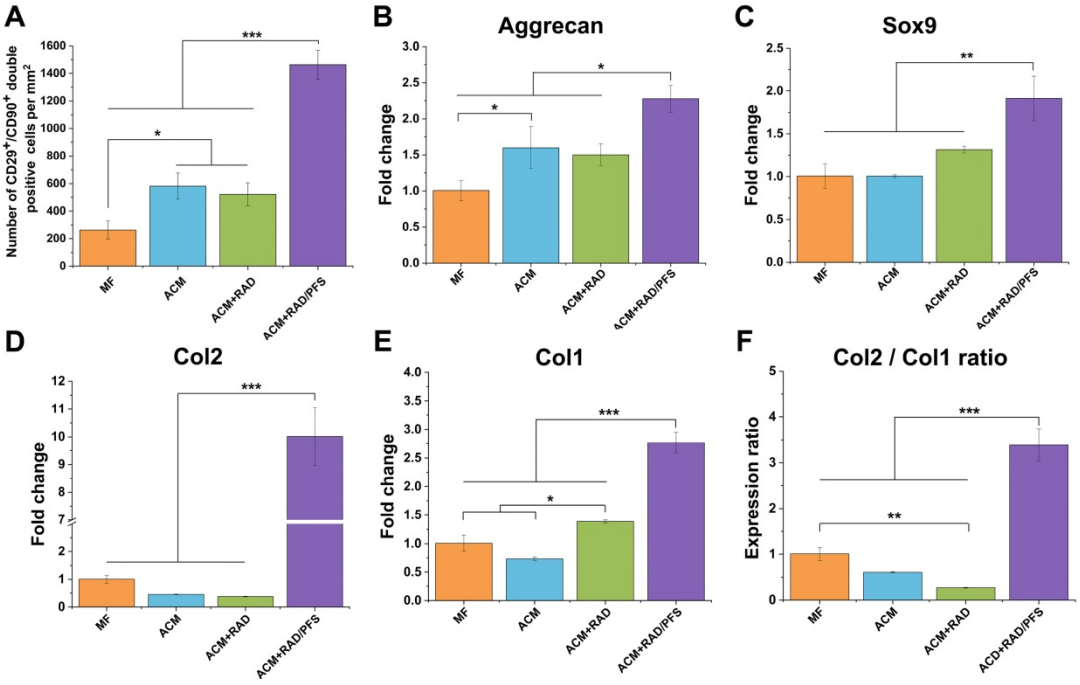

Figure 6. Quantification of recruited stem cells and gene expression examination for chondrogenic markers in newly formed tissue 7 days after surgery. (**A**) Quantification of cell number of CD29+/CD90+ double-positive cells per mm² (n = 3). Relative mRNA levels in tissue samples from all groups were tested for cartilage-specific markers, such as Aggrecan (**B**), Sox9 (**C**), and Col2 (**D**), as well as Col1 (osteogenic marker) (**E**) using qRT-PCR (n = 3). Values were normalized to GAPDH levels, and MF group was used as the control group. Mean ± SD; $^{*}p < 0.05$, $^{**}p < 0.01$ and $^{***}p < 0.001$.

The cartilage-associated genes, such as aggrecan, Sox9 and Col2, showed much higher expression in the ACM+RAD/PFS group than all other groups, particularly in the gene expression levels of Col2 (**Figure 6B-D**). As shown in **Figure 6D**, the gene expression levels of Col2 in the RAD/PFS group was about 10-fold higher than that of the MF control group ($p < 0.001$). There was no significant difference between MF, ACM and ACM+RAD groups in terms of the gene expression levels of Sox9 and Col2 (**Figure 6C-D**). Relative to MF and ACM groups, ACM+RAD group had higher, but not significant, mRNA levels of Sox9 (**Figure 6C**). These results suggest that recruited MSCs were efficiently differentiated into active chondrocytes within the ACM+RAD/PFS hydrogel system. For osteogenesis-associated genes, the gene expression levels of Col1 in the ACM+RAD/PFS group were slightly higher than those of the other three groups (**Figure 6E**). However, the strongly increased Col2:Col1 ratio demonstrated that the repaired matrix may progressively be composed mainly of the cartilage-specific Col2 (**Figure 6F**).

Micro-CT imaging and analysis

Because ACM+RAD/PFS composite scaffold showed great promise toward MSC homing and chondrogenesis *in vivo* at 7 days after implantation, we hypothesized that the composite scaffolds could facilitate endogenous repair in articular joints. In order to evaluate the therapeutic effects of ACM+RAD/PFS hydrogel composite for cartilage repair, ACM, ACM+RAD, and ACM+RAD/PFS scaffolds were implanted into full-thickness defects (3 mm in diameter × 1.5 mm depth) in rabbit joints for 3 months and 6 months, and the MF group was kept as a control.

Micro-CT reconstruction was performed of the articular joint samples of all groups at each timepoint (**Figure 7**). The 2D reconstruction images of coronal and sagittal cutting views were shown in **Figure 7A**, in which the green squares and arrows indicated the locations of the cartilage defects.

The defects in the ACM+RAD/PFS group were almost completely filled with well-integrated newly formed bone and cartilage-like tissues, with the cartilage layer being smooth and continuous at both 3 and 6 months post-surgery. However, there were still obvious unrepaired blank zones remaining (the part in the green squares) and a cracked cartilage layer in the other three groups at 3 months after operation (**Figure 7A**). Although the therapeutic outcome was improved at 6 months after implantation, the defects in the MF, ACM and ACM+RAD groups remained empty and discontinuous.

The quantitative data from micro-CT including bone mineral density (BMD) and bone volume fraction (BVF) also confirmed these results. As shown in **Figure 7B**, the BMD was statistically higher in the ACM+RAD/PFS group at both 3 months (234.1 ± 3.8 mg/mL) and 6 months (274.9 ± 6.3 mg/mL) than in

the other three groups (3 months: $p < 0.05$; 6 months: $p < 0.001$). The BMD in the ACM+RAD group (213.9 ± 6.2 mg/mL) was higher than that in the ACM alone group (197.5 ± 5.1 mg/mL) at 3 months post-operation, while there was no significant difference between the ACM group (237.7 ± 3.2 mg/mL) and ACM+RAD group (243.4 ± 3.7 mg/mL) at 6 months post-surgery. Although the BMD in the MF group was elevated, its value remained lowest among all groups at 3 months (149.5 ± 26.1 mg/mL) and 6 months (227.9 ± 3.3 mg/mL) after surgery (**Figure 7B**).

Moreover, the defects in the ACM+RAD/PFS group showed approximately 41.7% and 44.1% bone volume at 3 and 6 months after implantation, respectively (**Figure 7C**). The BVF values were similar among the ACM, ACM+RAD and ACM+RAD/PFS groups at the initial timepoint of 3 months. At 6 months post-surgery, the BVF in the ACM group was significantly lower than that in the ACM+RAD/PFS group ($p < 0.01$), while there was no significant difference between ACM and ACM+RAD groups (**Figure 7C**).

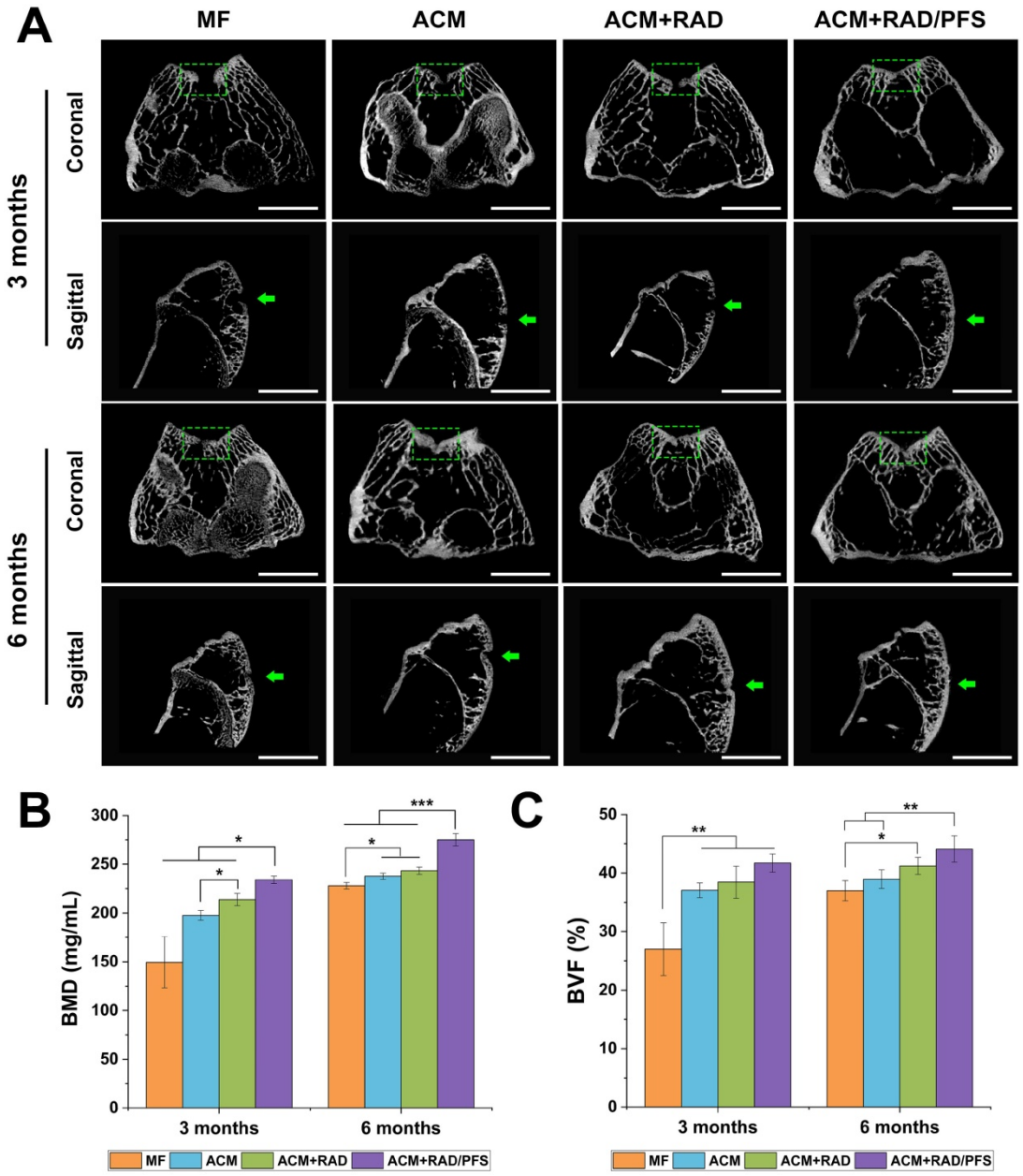

Figure 7. Micro-CT image analysis of the defects at 3 and 6 months post-surgery. (A) Representative coronal and sagittal 2D projection images of different groups. Scale bar = 2 cm. **(B-C)** Quantitative micro-CT analysis of regenerated bone within the defect space for bone mineral density (BMD) (B) and bone volume fraction (BVF) (C), in both trabecular volume of interest (VOI) and cartilage and cortical (C&C) VOI (n = 4). Mean ± SD; $^{*}p < 0.05$, $^{**}p < 0.01$ and $^{***}p < 0.001$.

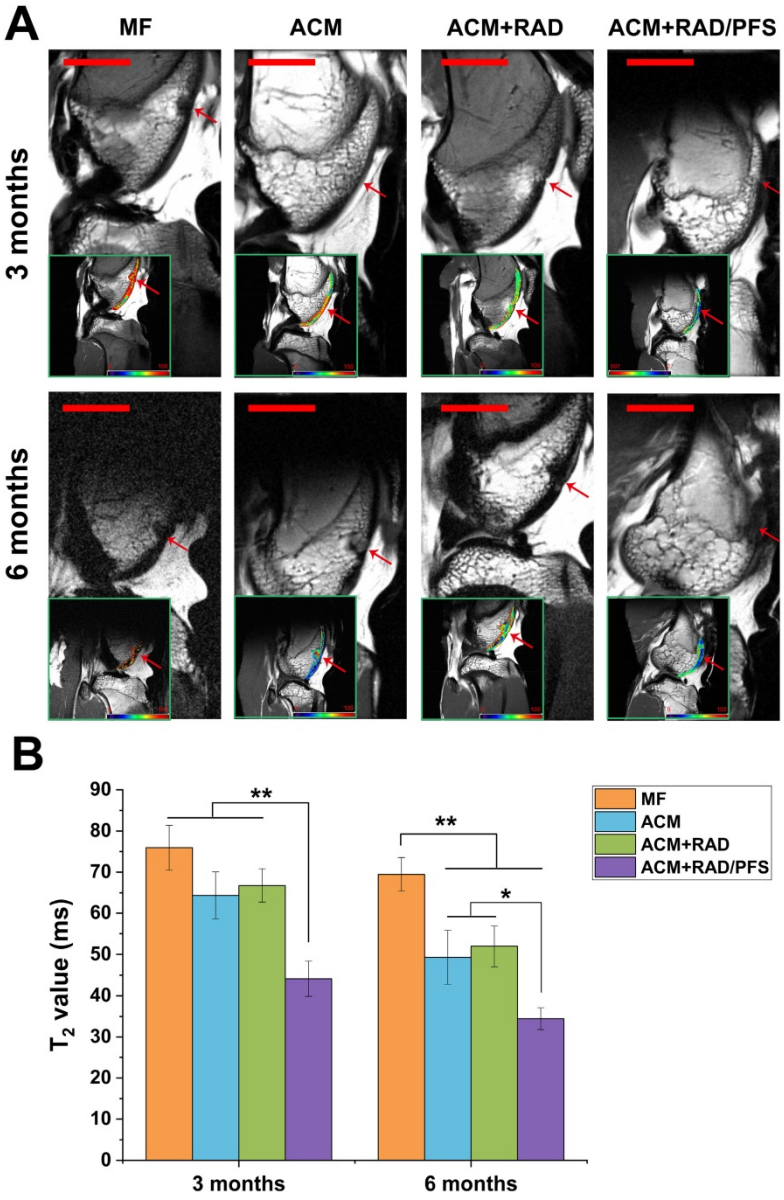

Figure 8. MRI detection and quantification of repaired knees. (A) MR imaging of repaired knees at 3 and 6 months post-surgery. The inset in the bottom left corner of each image shows the representative T_2 mapping images (red arrow, repaired sites of articular cartilage); pseudo-color scale, relaxation time (millisecond, ms). Scale bar = 2 cm. **(B)** T_2 relaxation time. Results are presented as the mean ± SD; n=3; $^{*}p < 0.05$, $^{**}p < 0.01$ and $^{***}p < 0.001$.

In summary, the micro-CT results demonstrated that the ACM+RAD/PFS composite scaffold possessed the optimal capacity for cartilage repair at the initial timepoint of 3 months post-surgery compared with the other groups.

MRI observations and quantification

The MRI images showed that the cartilage injuries in the MF group were poorly filled at 3 and 6 months after implantation (**Figure 8A**). The regenerated tissues in the ACM and ACM+RAD groups were partially filled with a rough surface at 6 months post-surgery. Only the ACM+RAD/PFS group showed a fully filled defect with a smooth surface, and its signal intensity of repaired tissue was similar to that of adjacent host cartilage at both 3 and 6 months after implantation (**Figure 8A**).

The regeneration of cartilage defects at 3 months and 6 months were quantitatively determined by T_2 mapping values. As shown in **Figure 8B**, the T_2 values in the cartilage defects of MF, ACM and ACM groups were significantly higher than that of the ACM+RAD/PFS group at 3 months after implantation ($p < 0.01$). At 6 months after surgery, the T_2 values in all groups were decreased. However, only the T_2 values of the repaired tissue in the ACM+RAD/PFS group (34.5 ± 2.6 ms) appeared almost the same as the signal values of adjacent native cartilage (31.2 ± 2.6) (**Figure 8B**).

Macroscopic evaluation of cartilage repair

Articular joint samples at 3 and 6 months post-surgery were harvested for gross evaluation of cartilage repair. As shown in **Figure 9A**, a visible defect was present in the MF group at 3 months after implantation. The defects of the ACM group appeared depressed and irregular compared with the host cartilage. Although the defects were mostly covered by new tissue in the ACM+RAD group, the boundaries with the surrounding normal cartilage were distinct. The ACM+RAD/PFS group exhibited the best performance among all groups after 3 months of treatment. The filling in the ACM+RAD/PFS group was more complete and uniform, as well as better integrated with the surrounding host cartilage (**Figure 9A**).

At 6 months post-surgery, cartilage defects were filled with improved repair tissues in all groups compared with those at 3 months. The defect in the MF group was thinnest, but a vacant position still existed. The defect in the ACM group was filled with uneven tissue, with distinct irregularity compared with the adjacent normal cartilage. The boundaries with the surrounding normal cartilage were gradually obscured in the ACM+RAD group at 6 months, but not as well as the ACM+RAD/PFS group (**Figure 9A**).

ICRS scoring showed similar results as macroscopic evaluation. As shown in **Figure 9B**, the ICRS macroscopic score was highest in the

ACM+RAD/PFS group at both 3 months (9.8 ± 1.0) and 6 months (10.4 ± 0.5) after implantation. The repaired tissues of the ACM+RAD/PFS group were considered as nearly normal (grade II) according to the ICRS overall repair assessment (**Table S3**). Though the ACM+RAD group had a higher score, it was not significantly different from the ACM alone group at each preselected timepoint. The scores were the worst in the MF group among these groups at both 3 and 6 months. Therefore, gross observation of repaired cartilage tissues showed that implantation in the ACM+RAD/PFS group could effectively promote regeneration of cartilage defects.

Histological assessment of repaired tissues

The repaired tissues were further analyzed histologically, and all groups were sliced for H&E and SR staining at each predetermined timepoint. The results of H&E staining are shown in **Figure S5**, and regional magnified images including the entire defected regions exhibit the microstructure and cellular distribution of repaired tissues (**Figure 10A, C, E, G**). At 3 months after surgery, the most disordered tissue was seen in the MF group, with severe surface irregularity compared with surrounding host cartilage. The defect in the ACM group was also filled with disordered tissue; the boundary between the repaired tissue and normal cartilage was apparent as well. For the ACM+RAD group, numerous fibroblast-like cells appeared at the top of regenerated tissue and were poorly organized. Different from the former groups, more highly organized chondrocyte-like cells were observed in the ACM+RAD/PFS group (**Figure 10G**). At 6 months after surgery, poorly organized tissues were still found in the MF, ACM and ACM+RAD groups. However, the defect in the ACM+RAD/PFS group was completely filled with cartilage-like tissue (i.e., most typical chondrocytes were arranged in columns and clusters), and a continuous surface as smooth as the surrounding host cartilage was observed (**Figure 10G**).

Sirius red staining was further used to visualize the pronounced collagen matrix deposited in the regenerated tissues of all groups. At 3 months post-surgery, the defects of the MF control group contained worn and disordered collagen fibers, with a rough surface (**Figure 10B**). Most Col1 with irregular organization was observed in the repaired tissue in the ACM and ACM+RAD groups, as compared with surrounding normal cartilage. At 6 months post-surgery, the ACM and ACM+RAD groups showed collagen fibers in parallel with the crack, with a rough edge (**Figure 10D, F**). Only the ACM+RAD/PFS group was rich in Col2, and the

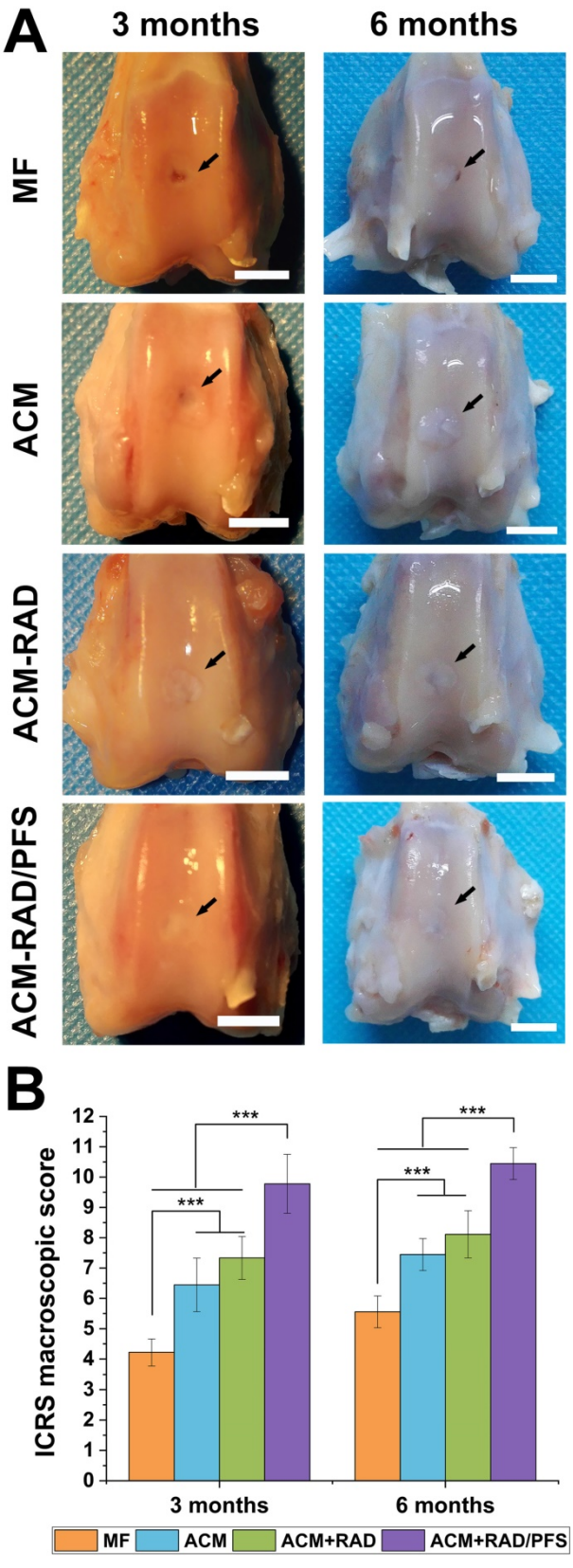

Figure 9. Macroscopic assessment of cartilage repair at 3 and 6 months post-surgery. (A) Representative images of the rabbit knee articular osteochondral defects (scale bars: 5 mm). The arrows indicate the original defect margin. **(B)** ICRS macroscopic evaluation scores. Results are presented as the mean ± SD; n=3; $^{*}p < 0.05$, $^{**}p < 0.01$ and $^{***}p < 0.001$.

collagen organization was consistent and arranged closely, which was similar to that of adjacent native cartilage at both 3 and 6 months after implantation (**Figure 10H**). These findings indicated that the ACM+RAD/PFS composite scaffold promoted chondrogenic differentiation of recruited MSCs and Col2 deposition during cartilage regeneration, whereas the other groups showed incomplete cartilage repair.

Cartilage-specific staining

Specific immunohistochemistry staining for Col2 revealed Col2 expression in the regenerated tissue of all groups. As shown in **Figure 11** and **Figure S6**, there were more chondrocytes and a higher content of Col2 in the ACM+RAD/PFS group than in the other three groups at surface and central areas at both 3 and 6 months after surgery, which confirmed the results of H&E and SR staining.

TB staining was further performed to detect the content of glycosaminoglycan (GAG), which is an important component of the cartilage ECM [45]. The repaired tissue in the MF group showed little staining with toluidine blue (**Figure 11B**), indicating poor GAG deposition, at each predetermined timepoint. At 6 months after surgery, the ACM and ACM+RAD groups showed higher content of GAG than that at 3 months (**Figure 11D, F**), but could not catch up with the ACM+RAD/PFS group. In the ACM+RAD/PFS group, the repair tissue displayed uniform TB staining, which was similar to the surrounding host cartilage at both 3 and 6 months after implantation (**Figure 11H**). These results demonstrated that the ACM+RAD/PFS group not only enhanced chondrogenesis, but increased Col2 secretion and cartilage-like ECM deposition *in vivo*.

In addition, the results of Safranin O/ Fast Green Staining after 6 months surgery are shown in **Figure S7**. A substantially higher amount of proteoglycan deposition was observed in the composite scaffold RAD/PFS, which displayed strong positive staining for Safranin O, as compared with the MF, ACM, and ACM+RAD groups, which mainly displayed fast green staining only.

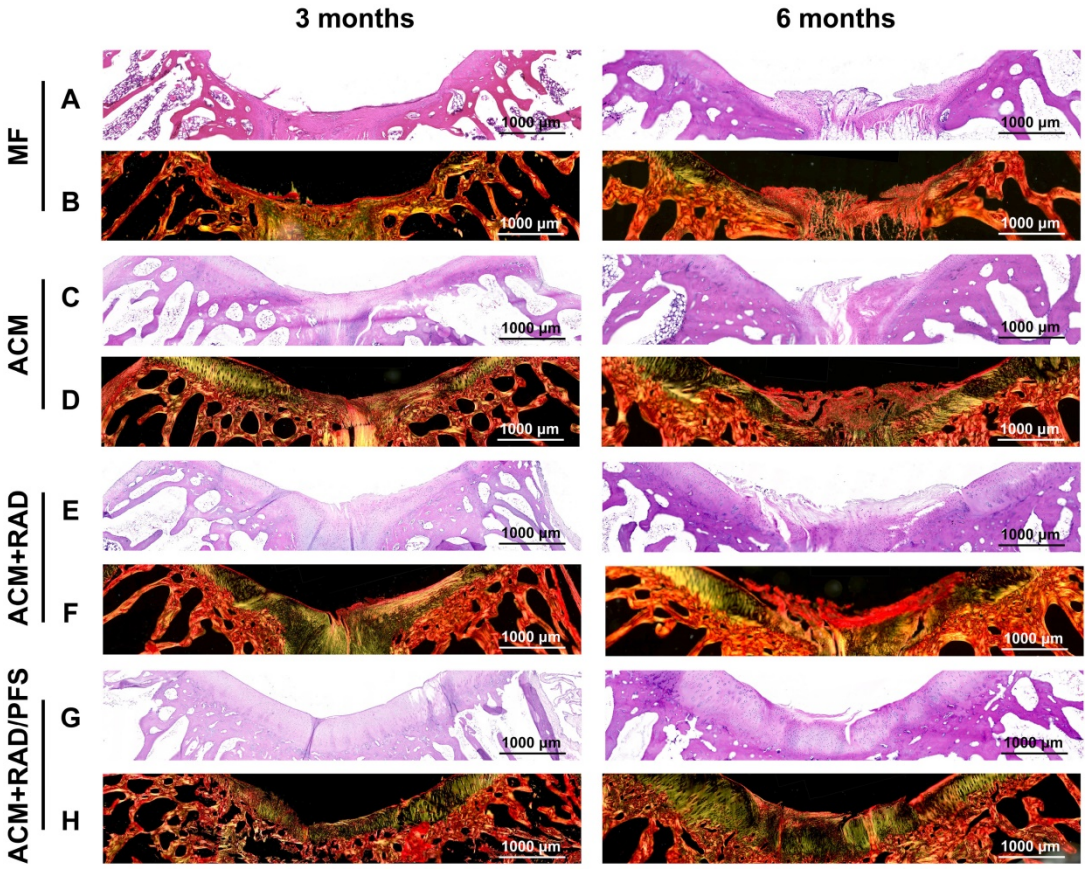

Figure 10. Histological assessment of repaired tissues. Representative images of H&E staining **(A, C, E, G)** and SR staining **(B, D, F, H)** of the osteochondral defects and repaired tissues at 3 and 6 months after surgery (n = 6).

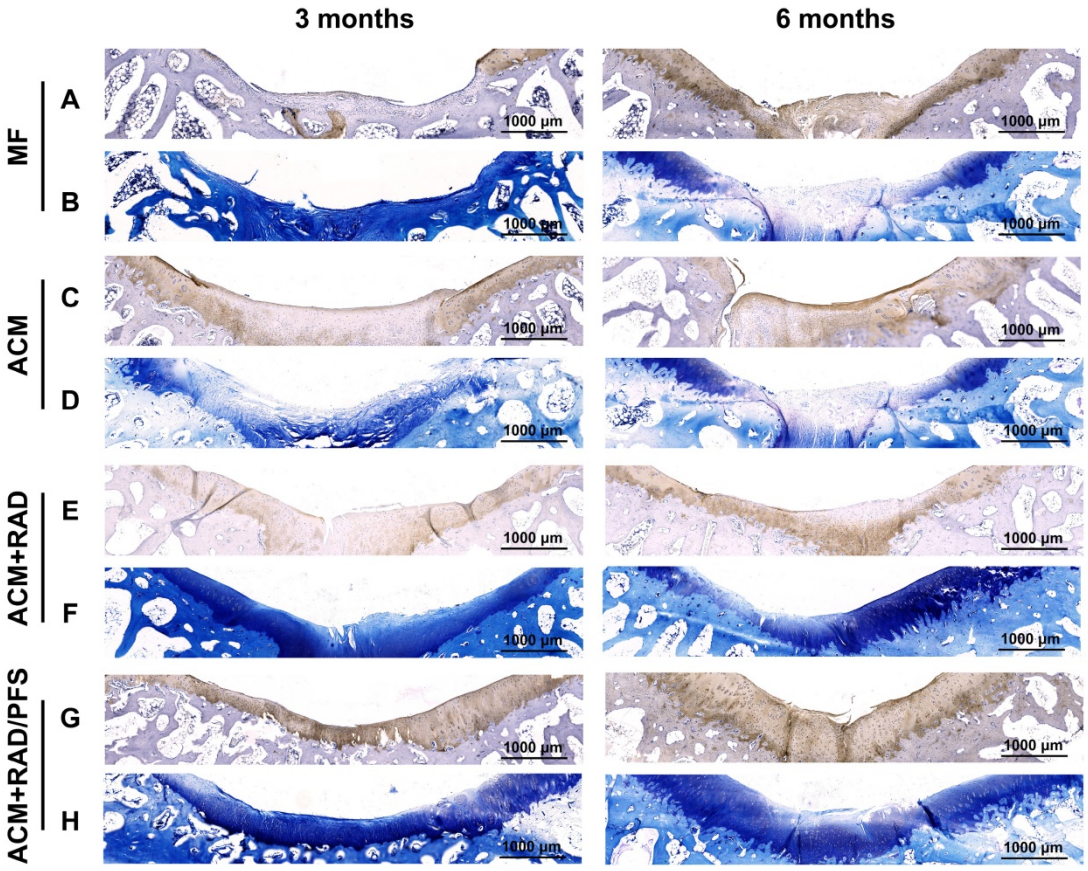

Figure 11. Cartilage-specific staining of repaired tissue. Representative images of Col2 staining **(A, C, E, G)** and TB staining **(B, D, F, H)** of the osteochondral defects and repaired tissues at 3 and 6 months after surgery (n = 6).

Histological scoring for the cartilage repair *in vivo*

Quantitative scoring of histological outcomes of cartilage repair at 6 months after implantation was performed using a histologic grading scale described by Wakitani [37]. The parameters for Wakitani grading scale consist of five parts: cell morphology, matrix staining, surface regularity, thickness of cartilage, and integration of new tissue with surrounding host cartilage (**Table S4**). The score ranges from 0 (normal cartilage) to 14 (most severe damage).

As shown in **Figure 12A**, the global histological scores (mean and (95% CI)) for the MF, ACM, ACM+RAD and ACM+RAD/PFS groups at 6 months were 9.7 ± 2.4 (8.5 to 10.8), 8.2 ± 2.0 (7.2 to 9.2), 6.7 ± 2.8 (5.3 to 8.1), and 4.4 ± 2.8 (3.0 to 5.8), respectively. The histological scoring results at 6 months showed significant difference between the ACM+RAD and ACM+RAD/PFS groups ($p < 0.05$), as well as the ACM and ACM+RAD/PFS groups ($p < 0.01$). **Figure 12B-F** show the score distributions for each parameter listed in **Table S4**. When evaluating the cell morphology of repaired tissue, more sections scored "hyaline cartilage" (score 0) in the ACM+RAD/PFS group, indicative of chondrogenic differentiation, than the other three groups (**Figure 12B**). Similar results have been shown in the detailed score distribution of other parameters (**Figure 12C-F**). These results demonstrated that the ACM+RAD/PFS group could effectively repair rabbit cartilage injury at 6 months after implantation.

Discussion

Stem cell homing has been considered as an alternative approach to cell delivery for tissue regeneration. This technique is readily applied, cost-effective, has no immunogenicity concerns and does not require *in vitro* culture of stem cells and their *in vivo* delivery. Rather, it relies on host cells *in situ* instead [46]. Therefore, constructing an ideal biomaterial scaffold that serves as a suitable artificial cell niche for recruiting and programing the functions of the recruited stem cells and the local tissue-specific cells is considered one of the key issues.

In this study, an oriented ACM scaffold that resembles the composition, microstructure, and mechanical behavior of natural cartilage tissue was applied because it has previously been shown to possess potential for cartilage repair [18, 47]. The ACM scaffold displayed pronounced biocompatibility and low immunogenicity inside the body because of

its natural sources. In addition, it has the paratactic columnar structure that could contribute to the columnar arrangement of chondrocytes. Nevertheless, the ACM scaffold lacks specific bioactivities to target endogenous stem cells and the clinical repair outcomes remain unsatisfactory.

In order to induce more stem cell migration into the defect during the first postoperative days, extra biochemical cues with a strong capacity for recruiting stem cells are essentially needed [4, 48]. It has been demonstrated that a BMHP, PFS, could induce homing of stem cells to the damage site and therefore has great therapeutic potential [20]. In this study, we employed PFS-functionalized self-assembling peptide to modify the oriented ACM scaffold. The composite hydrogel scaffold showed excellent moldability and tissue affinity that could easily fill the irregular shape of cartilage defects and adhere to surrounding tissues tightly. We found that the PFS-functionalized SAP hydrogel could promote rabbit MSCs proliferation, attachment and chondrogenic differentiation *in vitro* (**Figure 3** and **Figure 4**). Additionally, it was observed that the involvement of the PFS motif in the composite scaffold contributed to attracting more MSCs quickly with high efficiency.

However, recruiting abundant MSCs into the lesion site is not enough: further chondrogenic differentiation of the recruited cells is an essential requirement and plays a vital role in cartilage regeneration. The functionalized SAP hydrogel RAD/PFS has been proven to regulate and program certain types of stem cells, including neural stem cells (NSCs) [23], adipose stem cells (ASCs) [22], and endometrial-derived stromal cells [49]. Their behaviors of survival, proliferation, and differentiation were improved by RAD/PFS hydrogels. In this study, the results of qRT-PCR demonstrated that much higher expressions of chondrogenic genes (Sox9, aggreacan, and Col2) existed in the ACM+RAD/PFS composite scaffold compared with the other groups (**Figure 6B-D**).

The increased recruitment of endogenous stem cells and chondrogenic differentiation in the early stage by the composite scaffold should contribute to the late repair effects of injured cartilage. Micro-CT, MRI, and subsequent histological and immunohistochemistry staining at 3 and 6 months post-surgery confirmed the better therapeutic outcome after treatment with ACM+RAD/PFS composite scaffold. The content of GAGs and Col2, which are important components of the cartilage ECM, was much higher in the ACM+RAD/PFS group. Moreover, the defects of articular cartilage in the ACM+RAD/PFS group were fully filled with ordered cartilage-like tissue with a smooth surface, similar to the adjacent native cartilage. In addition, it was noted that the ACM and ACM+RAD groups showed no significant differences in many results, which indicated that RAD has insufficient contribution because of its lack of specific bioactivity.

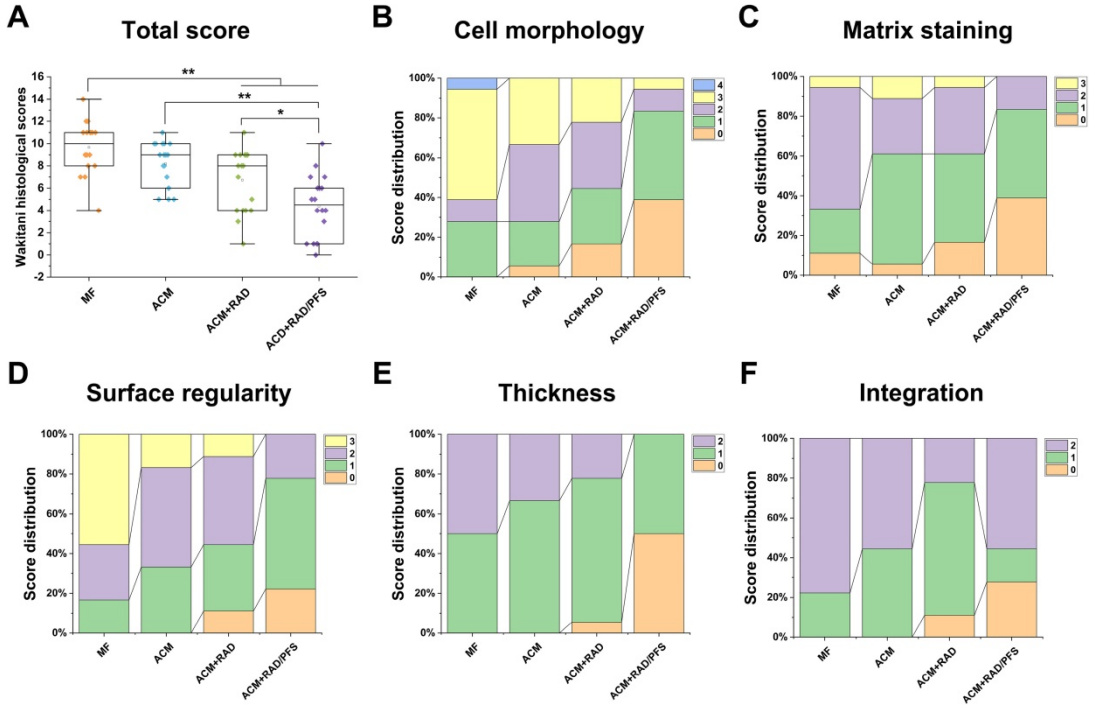

Figure 12. Histological score for the evaluation of osteochondral repair at 6 months after surgery. The histological total score **(A)** and its distribution for cell morphology **(B)**, matrix staining **(C)**, surface regularity **(D)**, thickness of cartilage **(E)**, and integration **(F)** are shown. Specific scoring criteria for each category are listed in **Table S4**. Results are presented as the mean ± SD; n=6; *$p < 0.05$, **$p < 0.01$ and ***$p < 0.001$.

The stability of the biochemical cues exhibited by an engineered tissue scaffold directly impacts its functionality and validity. Previous studies for cartilage regeneration by stem cells homing have focused on the application of chemokines and growth factors, such as transforming growth factor-β3 and -β1 [50, 51], stromal cell-derived factor-1 [52, 53], platelet-derived growth factor-AA [54], and their combined therapy [55]. However, their short half-life *in vivo* and deleterious side effects should be considered before widespread clinical use [56]. Recently, polypeptides are beginning to emerge as an alternative to the growth factors because peptides are more stable and are also safer, cheaper, and easier to control than chemokines and growth factors. Ao *et al*. identified an MSC-affinity peptide and successfully conjugated it to different scaffolds to enhance cell homing to stimulate cartilage regeneration [16, 17, 57, 58]. In our study, the ACM scaffold physically absorbed the self-assembling peptide functionalized with a bone marrow homing peptide PFS, which was then equilibrated to neutral conditions to initiate the gelation of SAP solution. The transparency of the composite scaffold increased in comparison with that of the pure ACM scaffold, indicating the increased water content of the SAP gels. Due to lacking of covalent interaction between SAP and ACM scaffold, the interactive bonding strength between them may not be very strong. Although chemical cross-linking could enhance their interactions, it would introduce toxic reagents and probably affect the effectiveness of bioactive polypeptides and the physicochemical properties of biomaterial scaffolds [59]. In this study, our results indicated that the MSCs could still be detected two weeks after surgery (**Figure S4**). The physically absorbed RAD/PFS could recruit more MSCs, which contributed to the better repair and cartilage regeneration in the ACM+RAD/PFS group.

The scaffolds used in this study showed good *in vivo* biodegradability. The ACM scaffold is made of natural articular cartilage ECM, which had good *in vivo* biodegradation [18, 19]. SAP hydrogels have been widely used in tissue engineering and regenerative medicine, were stable in cell culture medium for several weeks, but showed good degradation *in vivo* because of the complex microenvironment with changing pH, ionic strength, and enzymes [60-62]. In this study, histological examination indicated that the scaffolds of ACM and ACM+SAP underwent degradation and were replaced by newly formed cartilage tissues within 3 months.

Although the desired therapeutic outcomes of cartilage injury were achieved, the repaired cartilage-like tissues of the ACM+RAD/PFS group are not as good as normal cartilage. More biochemical and biophysical regulatory signals should be developed to modify scaffolds to assist full regeneration. In addition, the molecular and cellular mechanisms underlying stem cell homing to the defects of cartilage injury are still not precisely understood. Therefore, further studies are needed to clarify these questions clearly.

In summary, the damage site of articular cartilage was repaired well by an ACM+RAD/PFS composite scaffold that quickly recruited more endogenous stem cells and promoted their chondrogenic differentiation remarkably. The present strategy may provide a feasible method for repairing damaged tissues without cell transplantation. These findings suggest that the implantation of composite hydrogel scaffolds for cartilage injury could potentially be explored in the clinic to treat patients with osteoarthritis, rheumatoid arthritis, or osteonecrosis.

Conclusion

In this study, we developed and fabricated a composite hydrogel scaffold ACM+RAD/PFS with oriented structure and stem cell homing activity. Its potential for articular cartilage regeneration in a rabbit model was evaluated. Our results demonstrated that the composite scaffold enhanced endogenous stem cell homing and accelerated the process of chondrogenesis compared to microfracture or control scaffolds. Therefore, this scaffold has great promise in cartilage tissue engineering without cell transplantation.

Abbreviations

3D: three dimensional; ACM: acellular cartilage matrix; AFM: atomic force microscopy; ANOVA: analysis of variance; BMD: bone mineral density; BMHP: bone marrow homing peptide; BVF: bone volume fraction; CD: circular dichroism; Col1: type I collagen; Col2: type II collagen; ECM: extracellular matrix; GAGs: glycosaminoglycans; H&E: hematoxylin and eosin; ICRS: International Cartilage Repair Society; micro-CT: microcomputed tomography; MRI: magnetic resonance imaging; MSCs: mesenchymal stem cells; PLA: poly(lactic acid); PLGA: poly(lactic-co-glycollic acid); qRT-PCR: quantitative real-time polymerase chain reaction; SAP: self-assembling peptide; SEM: scanning electron microscopy; SR: Sirius red; TB: toluidine blue; VOI: volume of interest.

Acknowledgements

We acknowledge financial support from the National Natural Science Foundation of China (Nos. 31771056, 81572148, 81772319), the Tsinghua

University Initiative Scientific Research Program (No. 20161080091), the 111 Project (No. B17026), Beijing Municipal Science and Technology Project (Z161100005016059), the People's Liberation Army 12th 5-year plan period project (BWS11J025), the Project of Translational Medicine of Chinese PLA General Hospital (2016TM-020). Thanks are given to Xiaoqing Yan from Beijing Tsinghua Changgung Hospital, Zijiao Zhang from Dalian Medical University, and Jinjin Zhu from Ningbo University for their kind help with histological scoring. We thank Haitao Fu in the institute of Orthopedics, Chinese PLA General Hospital for generous help with animal experiments, and Tao Wu at the school of medicine, Tsinghua University for help with agarose gel electrophoresis. We also would like to thank Yue Sun at Center of Biomedical Analysis, Tsinghua University for help with confocal microscopy. Finally, we thank Hannah Pearce from Rice University for her assistance in the preparation of the manuscript.

Supplementary Material

Supplementary figures and tables.
http://www.thno.org/v08p5039s1.pdf

Competing Interests

The authors have declared that no competing interest exists.

References

1. Huey DJ, Hu JC, Athanasiou KA. Unlike bone, cartilage regeneration remains elusive. Science. 2012; 338: 917-21.
2. Hunziker EB. Articular cartilage repair: basic science and clinical progress. A review of the current status and prospects. Osteoarthritis Cartilage. 2002; 10: 432-63.
3. Jackson DW, Simon TM, Aberman HM. Symptomatic articular cartilage degeneration: the impact in the new millennium. Clin Orthop Relat Res (1976-2007). 2001; 391: S14-S25.
4. Koga H, Engebretsen L, Brinchmann JE, Muneta T, Sekiya I. Mesenchymal stem cell-based therapy for cartilage repair: a review. Knee Surg Sports Traumatol Arthrosc. 2009; 17: 1289-97.
5. Chen F-M, Wu L-A, Zhang M, Zhang R, Sun H-H. Homing of endogenous stem/progenitor cells for *in situ* tissue regeneration: Promises, strategies, and translational perspectives. Biomaterials. 2011; 32: 3189-209.
6. Yin Y, Li X, He XT, Wu RX, Sun HH, Chen FM. Leveraging stem cell homing for therapeutic regeneration. J Dent Res. 2017; 96: 601-9.
7. Mao JJ. Stem-cell-driven regeneration of synovial joints. Biol Cell. 2005; 97: 289-301.
8. Steadman JR, Rodkey WG, Rodrigo JJ. Microfracture: surgical technique and rehabilitation to treat chondral defects. Clin Orthop Relat Res. 2001; 391: S362.
9. Gobbi A, Karnatzikos G, Kumar A. Long-term results after microfracture treatment for full-thickness knee chondral lesions in athletes. Knee Surg Sports Traumatol Arthrosc. 2014; 22: 1986-96.
10. Gomoll AH, Madry H, Knutsen G, van Dijk N, Seil R, Brittberg M, et al. The subchondral bone in articular cartilage repair: current problems in the surgical management. Knee Surg Sports Traumatol Arthrosc. 2010; 18: 434-47.
11. Asik M, Ciftci F, Sen C, Erdil M, Atalar A. The microfracture technique for the treatment of full-thickness articular cartilage lesions of the knee: midterm results. Arthroscopy. 24: 1214-20.
12. Lee KB, Wang VT, Chan YH, Hui JH. A novel, minimally-invasive technique of cartilage repair in the human knee using arthroscopic microfracture and injections of mesenchymal stem cells and hyaluronic acid--a prospective comparative study on safety and short-term efficacy. Ann Acad Med Singapore. 2012; 41: 511-7.
13. A. SR, F. WJ, Diego C, I. CA. Chondrogenic differentiation of mesenchymal stem cells: challenges and unfulfilled expectations. Tissue Eng Part B Rev. 2014; 20: 596-608.
14. Gomoll AH. Microfracture and augments. J Knee Surg. 2012; 25: 9-15.
15. Khan IM, Gilbert SJ, Singhrao SK, Duance VC, Archer CW. Cartilage integration: evaluation of the reasons for failure of integration during cartilage repair. A review. Eur Cell Mater. 2008; 16: 26-39.
16. Meng Q, Man Z, Dai L, Huang H, Zhang X, Hu X, et al. A composite scaffold of MSC affinity peptide-modified demineralized bone matrix particles and chitosan hydrogel for cartilage regeneration. Sci Rep. 2015; 5: 17802.
17. Huang H, Zhang X, Hu X, Shao Z, Zhu J, Dai L, et al. A functional biphasic biomaterial homing mesenchymal stem cells for *in vivo* cartilage regeneration. Biomaterials. 2014; 35: 9608-19.
18. Zheng X, Yang F, Wang S, Lu S, Zhang W, Liu S, et al. Fabrication and cell affinity of biomimetic structured PLGA/articular cartilage ECM composite scaffold. J Mater Sci Mater Med. 2011; 22: 693-704.
19. Yang Q, Peng J, Guo Q, Huang J, Zhang L, Yao J, et al. A cartilage ECM-derived 3-D porous acellular matrix scaffold for *in vivo* cartilage tissue engineering with PKH26-labeled chondrogenic bone marrow-derived mesenchymal stem cells. Biomaterials. 2008; 29: 2378-87.
20. Nowakowski GS, Dooner MS, Valinski HM, Mihaliak AM, Quesenberry PJ, Becker PS. A specific heptapeptide from a phage display peptide library homes to bone marrow and binds to primitive hematopoietic stem cells. Stem Cells. 2004; 22: 1030-8.
21. Cao F-Y, Yin W-N, Fan J-X, Zhuo R-X, Zhang X-Z. A novel function of BMHP1 and cBMHP1 peptides to induce the osteogenic differentiation of mesenchymal stem cells. Biomater Sci. 2015; 3: 345-51.
22. Chen Y, Lu J, Chen B, Wang S, Rana D, Ramalingam M, et al. PFS-functionalized self-assembling peptide hydrogel for the maintenance of human adipose stem cell *in vitro*. J Biomater Tissue Eng. 2017; 7: 943-51.
23. Gelain F, Bottai D, Vescovi A, Zhang S. Designer self-assembling peptide nanofiber scaffolds for adult mouse neural stem cell 3-Dimensional cultures. PLoS One. 2006; 1: e119.
24. Kisiday J, Jin M, Kurz B, Hung H, Semino C, Zhang S, et al. Self-assembling peptide hydrogel fosters chondrocyte extracellular matrix production and cell division: Implications for cartilage tissue repair. Proc Natl Acad Sci U S A. 2002; 99: 9996-10001.
25. Liu J, Song H, Zhang L, Xu H, Zhao X. Self-assembly-peptide hydrogels as tissue-engineering scaffolds for three-dimensional culture of chondrocytes *in vitro*. Macromol Biosci. 2010; 10: 1164-70.
26. Erickson IE, Huang AH, Chung C, Li RT, Burdick JA, Mauck RL. Differential maturation and structure–function relationships in mesenchymal stem cell- and chondrocyte-seeded hydrogels. Tissue Eng Part A. 2009; 15: 1041-52.
27. Lu J, Sun X, Yin H, Shen X, Yang S, Wang Y, et al. A neurotrophic peptide-functionalized self-assembling peptide nanofiber hydrogel enhances rat sciatic nerve regeneration. Nano Res. 2018; 11: 4599-4613.
28. Chau Y, Luo Y, Cheung ACY, Nagai Y, Zhang S, Kobler JB, et al. Incorporation of a matrix metalloproteinase-sensitive substrate into self-assembling peptides – A model for biofunctional scaffolds. Biomaterials. 2008; 29: 1713-9.
29. Huang H, Zhang X, Hu X, Shao Z, Zhu J, Dai L, et al. A functional biphasic biomaterial homing mesenchymal stem cells for *in vivo* cartilage regeneration. Biomaterials. 2014; 35: 9608-19.
30. Livak KJ, Schmittgen TD. Analysis of relative gene expression data using real-time quantitative PCR and the 2−ΔΔCT method. Methods. 2001; 25: 402-8.
31. Luo Z, Jiang L, Xu Y, Li H, Xu W, Wu S, et al. Mechano growth factor (MGF) and transforming growth factor (TGF)-β3 functionalized silk scaffolds enhance articular hyaline cartilage regeneration in rabbit model. Biomaterials. 2015; 52: 463-75.
32. Dao TT, Vu NB, Pham LH, Van Gia L, Le HT, Phi LT, et al. *In vitro* production of cartilage tissue from rabbit bone marrow-derived mesenchymal stem cells and polycaprolactone scaffold. In: Adv Exp Med Biol. Springer, Boston, MA; 2018: 1-16.
33. Tan SL, Ahmad TS, Selvaratnam L, Kamarul T. Isolation, characterization and the multi-lineage differentiation potential of rabbit bone marrow-derived mesenchymal stem cells. J Anat. 2013; 222: 437-50.
34. Yin H, Wang Y, Sun Z, Sun X, Xu Y, Li P, et al. Induction of mesenchymal stem cell chondrogenic differentiation and functional cartilage microtissue formation for *in vivo* cartilage regeneration by cartilage extracellular matrix-derived particles. Acta Biomater. 2016; 33: 96-109.
35. Mamisch TC, Hughes T, Mosher TJ, Mueller C, Trattnig S, Boesch C, et al. T2 star relaxation times for assessment of articular cartilage at 3 T: a feasibility study. Skeletal Radiol. 2012; 41: 287-92.
36. van den Borne MPJ, Raijmakers NJH, Vanlauwe J, Victor J, de Jong SN, Bellemans J, et al. International Cartilage Repair Society (ICRS) and Oswestry macroscopic cartilage evaluation scores validated for use in Autologous Chondrocyte Implantation (ACI) and microfracture. Osteoarthritis Cartilage. 2007; 15: 1397-402.
37. Wakitani S, Goto T, Pineda SJ, Young RG, Mansour JM, Caplan AI, et al. Mesenchymal cell-based repair of large, full-thickness defects of articular cartilage. JBJS. 1994; 76: 579-92.
38. Kolf CM, Cho E, Tuan RS. Mesenchymal stromal cells: Biology of adult mesenchymal stem cells: regulation of niche, self-renewal and differentiation. Arthritis Res Ther. 2007; 9: 204.
39. Susanne K, Hermann E, Johannes S, Harald K, Karen B. Comparative analysis of mesenchymal stem cells from bone marrow, umbilical cord blood, or adipose tissue. Stem Cells. 2006; 24: 1294-301.
40. Deng J, She R, Huang W, Dong Z, Mo G, Liu B. A silk fibroin/chitosan scaffold in combination with bone marrow-derived mesenchymal stem cells to repair cartilage defects in the rabbit knee. J Mater Sci Mater Med. 2013; 24: 2037-46.

41. Sik-Loo T, Sara AT, Lakshmi S, Tunku K. Isolation, characterization and the multi-lineage differentiation potential of rabbit bone marrow-derived mesenchymal stem cells. J Anat. 2013; 222: 437-50.
42. Yang J, Chen X, Yuan T, Yang X, Fan Y, Zhang X. Regulation of the secretion of immunoregulatory factors of mesenchymal stem cells (MSCs) by collagen-based scaffolds during chondrogenesis. Mater Sci Eng C. 2017; 70: 983-91.
43. Li TZ, Kim JH, Cho HH, Lee HS, Kim KS, Lee SW, et al. Therapeutic potential of bone-marrow-derived mesenchymal stem cells differentiated with growth-factor-free coculture method in liver-injured rats. Tissue Eng Part A. 2010; 16: 2649-59.
44. Hee KS, Woojune H, Eun KJ, Jeong MH, Sukwha K, Sook MH, et al. Self-assembling peptide nanofibers coupled with neuropeptide substance P for bone tissue engineering. Tissue Eng Part A. 2015; 21: 1237-46.
45. Gao Y, Liu S, Huang J, Guo W, Chen J, Zhang L, et al. The ECM-cell interaction of cartilage extracellular matrix on chondrocytes. Biomed Res Int. 2014; 2014: 8.
46. Wu RX, Yin Y, He XT, Li X, Chen FM. Engineering a cell Home for stem cell homing and accommodation. Adv Biosyst. 2017; 1: 1700004.
47. Zhang Y, Liu S, Guo W, Wang M, Hao C, Gao S, et al. Human umbilical cord Wharton's jelly mesenchymal stem cells combined with an acellular cartilage extracellular matrix scaffold improve cartilage repair compared with microfracture in a caprine model. Osteoarthritis Cartilage. 2018; 26: 954-965.
48. Steadman JR, Briggs KK, Rodrigo JJ, Kocher MS, Gill TJ, Rodkey WG. Outcomes of microfracture for traumatic chondral defects of the knee: Average 11-year follow-up. Arthroscopy. 2003; 19: 477-84.
49. Tavakol S, Saber R, Hoveizi E, Aligholi H, Ai J, Rezayat SM. Chimeric self-assembling nanofiber containing bone marrow homing peptide's motif induces motor neuron recovery in animal model of chronic spinal cord injury; an *in vitro* and *in vivo* investigation. Mol Neurobiol. 2016; 53: 3298-308.
50. Lee CH, Cook JL, Mendelson A, Moioli EK, Yao H, Mao JJ. Regeneration of the articular surface of the rabbit synovial joint by cell homing: a proof of concept study. Lancet. 2010; 376: 440-8.
51. Zhou T, Li X, Li G, Tian T, Lin S, Shi S, et al. Injectable and thermosensitive TGF-β1-loaded PCEC hydrogel system for *in vivo* cartilage repair. Sci Rep. 2017; 7: 10553.
52. Chen P, Tao J, Zhu S, Cai Y, Mao Q, Yu D, et al. Radially oriented collagen scaffold with SDF-1 promotes osteochondral repair by facilitating cell homing. Biomaterials. 2015; 39: 114-23.
53. Yu Y, Brouillette MJ, Seol D, Zheng H, Buckwalter JA, Martin JA. Use of recombinant human stromal cell–derived factor 1α–loaded fibrin/hyaluronic acid hydrogel networks to achieve functional repair of full-thickness bovine articular cartilage via homing of chondrogenic progenitor cells. Arthritis Rheumatol. 2015; 67: 1274-85.
54. Lee JM, Ryu JH, Kim EA, Jo S, Kim B-S, Lee H, et al. Adhesive barrier/directional controlled release for cartilage repair by endogenous progenitor cell recruitment. Biomaterials. 2015; 39: 173-81.
55. Mendelson A, Frank E, Allred C, Jones E, Chen M, Zhao W, et al. Chondrogenesis by chemotactic homing of synovium, bone marrow, and adipose stem cells *in vitro*. FASEB J. 2011; 25: 3496-504.
56. Mitchell AC, Briquez PS, Hubbell JA, Cochran JR. Engineering growth factors for regenerative medicine applications. Acta Biomater. 2016; 30: 1-12.
57. Meng Q, Hu X, Huang H, Liu Z, Yuan L, Shao Z, et al. Microfracture combined with functional pig peritoneum-derived acellular matrix for cartilage repair in rabbit models. Acta Biomater. 2017; 53: 279-92.
58. Shao Z, Zhang X, Pi Y, Wang X, Jia Z, Zhu J, et al. Polycaprolactone electrospun mesh conjugated with an MSC affinity peptide for MSC homing *in vivo*. Biomaterials. 2012; 33: 3375-87.
59. Balcão VM, Vila MMDC. Structural and functional stabilization of protein entities: state-of-the-art. Adv Drug Deliv Rev. 2015; 93: 25-41.
60. Wu X, He L, Li W, Li H, Wong W-M, Ramakrishna S, et al. Functional self-assembling peptide nanofiber hydrogel for peripheral nerve regeneration. Regen Biomater. 2017; 4: 21-30.
61. Liu X, Wang X, Horii A, Wang X, Qiao L, Zhang S, et al. *In vivo* studies on angiogenic activity of two designer self-assembling peptide scaffold hydrogels in the chicken embryo chorioallantoic membrane. Nanoscale. 2012; 4: 2720-7.
62. Cheng T-Y, Chen M-H, Chang W-H, Huang M-Y, Wang T-W. Neural stem cells encapsulated in a functionalized self-assembling peptide hydrogel for brain tissue engineering. Biomaterials. 2013; 34: 2005-16.